

4-2017

# The Effect of Pressure and Interstitial Substitution on the Electronic Properties of Molybdenum Disulfide Mos<sub>2</sub>

Wadha Khalifa Salem Rashed AlFalasi

Follow this and additional works at: [https://scholarworks.uaeu.ac.ae/phys\\_theses](https://scholarworks.uaeu.ac.ae/phys_theses)

Part of the [Physics Commons](#)

---

## Recommended Citation

Rashed AlFalasi, Wadha Khalifa Salem, "The Effect of Pressure and Interstitial Substitution on the Electronic Properties of Molybdenum Disulfide Mos<sub>2</sub>" (2017). *Physics Theses*. 2.  
[https://scholarworks.uaeu.ac.ae/phys\\_theses/2](https://scholarworks.uaeu.ac.ae/phys_theses/2)

This Thesis is brought to you for free and open access by the Physics at Scholarworks@UAEU. It has been accepted for inclusion in Physics Theses by an authorized administrator of Scholarworks@UAEU. For more information, please contact [fadl.musa@uaeu.ac.ae](mailto:fadl.musa@uaeu.ac.ae).

**UAEU**



جامعة الإمارات العربية المتحدة  
United Arab Emirates University

United Arab Emirates University

College of Science

Department of Physics

THE EFFECT OF PRESSURE AND INTERSTITIAL SUBSTITUTION  
ON THE ELECTRONIC PROPERTIES OF MOLYBDENUM  
DISULFIDE  $\text{MoS}_2$

Wadha Khalifa Salem Rashed AlFalasi

This thesis is submitted in partial fulfilment of the requirements for the degree of  
Master of Science in Physics

Under the Supervision of Professor Noureddine Amrane

April 2017

### Declaration of Original Work

I, Wadha Khalifa Salem Rashed AlFalasi, the undersigned, a graduate student at the United Arab Emirates University (UAEU), and the author of this thesis entitled "*The Effect of Pressure and Interstitial Substitution on the Electronic Properties of Molybdenum Disulfide MoS<sub>2</sub>*", hereby, solemnly declare that this thesis is my own original research work that has been done and prepared by me under the supervision of Professor Nouredine Amrane, in the College of Science at UAEU. This work has not previously been presented nor published, or formed the basis for the award of any academic degree, diploma or a similar title at this or any other university. Any materials borrowed from other sources (whether published or unpublished) and relied upon or included in my thesis have been properly cited and acknowledged in accordance with appropriate academic conventions. I further declare that there is no potential conflict of interest with respect to the research, data collection, authorship, presentation and/or publication of this thesis.

Student's Signature: Wadha

Date: 14th - May - 2017

Copyright © 2017 Wadha Khalifa Salem Rashed AlFalasi  
All Rights Reserved

## Advisory Committee

1) Advisor: Prof. Nouredine Amrane

Title: Professor

Department of Physics

College of Science

2) Co-advisor: Prof. Maamar Benkraouda

Title: Professor

Department of Physics

College of Science

3) Co-advisor: Prof. Naser Qamhieh

Title: Professor

Department of Physics

College of Science

## Approval of the Master Thesis

This Master Thesis is approved by the following Examining Committee Members:

- 1) Advisor (Committee Chair): Noureddine Amrane

Title: Professor

Department of Physics

College of Science

Signature  \_\_\_\_\_

Date 30/4/2017

- 2) Member: Saleh Thaker Mahmoud

Title: Professor

Department of Physics

College of Science

Signature \_\_\_\_\_ 

Date 30/4/2017

- 3) Member (External Examiner): Kais Daoudi

Title: Assistant professor

Department of applied physics

Institution: University of Sharjah, UAE

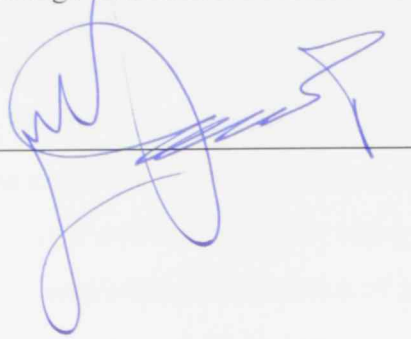
Signature \_\_\_\_\_ 

Date 30-04-2017

This Master Thesis is accepted by:

Dean of the College of Science: Professor Ahmed Murad

Signature

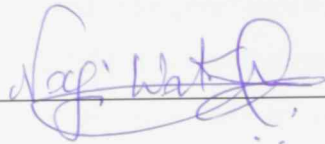


Date

14/5/2017

Dean of the College of Graduate Studies: Professor Nagi T. Wakim

Signature



Date

14/5/2017

## Abstract

Molybdenum disulfide has some of graphene's properties but has an edge over graphene as this new 2D nanomaterial has a band gap in its electronic structure, which is absent in graphene. The purpose of this thesis is to study the electronic properties of the promising Molybdenum Disulfide ( $\text{MoS}_2$ ) material in its bulk and monolayer forms by undertaking a systematic theoretical approach. We will mainly study the band gap, the density of states and the electronic charge distribution which is considered as the most important electronic characteristics of semiconductors.

In this study, the density functional theory (DFT) – implemented in WIEN2k and VASP- is used. The generalized gradient approximation (GGA), Modified Becke-Johnson and Hybrid functional approximation are used for the exchange–correlation potential. Band structure, density of states and band gap pressure coefficients are calculated.  $\text{WSe}_2$  –  $\text{MoS}_2$  heterostructure and the effect of impurities are covered in this study.

The study matched the experimental results, the band gap of molybdenum disulfide increases with decreasing the number of layers and it shifts from an indirect band gap to a direct band gap when a monolayer  $\text{MoS}_2$  is formed. The pressure effect found in this study is consistent with the experiments and supports the idea of changing the electrical phase of  $\text{MoS}_2$  with pressure (from semiconductor to metallic phase).

This study shows that  $\text{MoS}_2$  is an excellent candidate in electronics industry along with its great applications as lubricant, Transistors and composite applications.

**Keywords:** Molybdenum disulfide, 2D material, density functional theory, electronic properties.



## Title and Abstract (in Arabic)

### دراسة أثر الضغط والشوائب على الخصائص الالكترونية لثاني كبريتيد الموليبدينيوم

#### الملخص

يعد ثاني كبريتيد الموليبدينيوم ( $\text{MoS}_2$ ) من أكثر المواد استقطابا لاهتمام العلماء لأنه يشارك الجرافين بعض خصائصه ولكن يختلف عنه لوجود فجوة بين مستويات طاقة الالكترون في الذرة. الهدف من هذه الأطروحة هو دراسة الخصائص الالكترونية لثاني كبريتيد الموليبدينيوم. سيتم استخدام نظرية الدالة الوظيفية للكثافة (Density functional theory DFT) لفهم ودراسة البنية والخصائص الالكترونية التي تعتبر كثافة الالكترونات هي الأساس لدراسة خصائص المجموعة. بالاستعانة بتقريب الانحدار المعمم (Generalized Gradient Approximation) و تقريب بيك – جونسون المعدل, (Modified Becke-Johnson) سيتم حساب جهد التبادل – الارتباط الكامن بين الالكترونات. باستخدام التقريبات السابقة الذكر سيتم حساب فجوة الطاقة بين الالكترونات و كثافة المستويات (Density of states)، بالإضافة إلى دراسة تأثير الضغط على الخصائص الالكترونية، بالإضافة إلى دراسة التغييرات التي قد تحصل على ثاني كبريتيد الموليبدينيوم عند وضعه مع تنجستن ثنائي السيلينيوم  $\text{WSe}_2$  أو عند إضافة شوائب.

أظهرت الدراسة أن الفجوة الالكترونية تزيد مع تقليص عدد طبقات المادة المدروسة كما أن الفجوة تتحول من كونها مباشرة (Direct band gap) إلى كونها غير مباشرة (Indirect band gap) عند الانتقال من عدة طبقات (Bulk) إلى طبقة واحدة فقط ( $\text{Monolayer MoS}_2$ ). أوضحت دراسة تأثير الضغط تغيير في الخصائص الالكترونية للمادة حيث أنها تبدي خصائص مائلة إلى الموصلات عند زيادة الضغط عليها.

**مفاهيم البحث الرئيسية:** ثاني كبريتيد الموليبدينيوم، نظرية الدالة الوظيفية، الخصائص الالكترونية.

## Acknowledgements

I express my deepest gratitude to Prof. Nouredine Amrane for his aspiring guidance, precious constructive advice, friendly criticism and lots of his time. My thanks go to both Prof. Usama AlKhawaja, the head of the Physics department, and Prof. Abdessamad Abada, the Master program coordinator, for their support and guidance throughout the courses of this program. Special thanks go to Prof. Maamar Benkraouda who provided insight and expertise to interpret our result and asses them.

I am using this opportunity to thank all members of the Physics department for introducing me to the exciting field of physics at the United Arab Emirates University and providing me with the best learning experience that I would ever get. Furthermore, I would, with much appreciation, like to acknowledge the crucial role of Dr. Xiaoping Han for his valuable assistance with the VASP package.

I would also like to express my warm thanks to my beloved family and friends, who are surely more thankful than I am that this journey came to a beautiful end.

## Dedication

*To my mother, whom I owe everything in my life. My Father, who always see the best in me. Finally, to my husband, for his extreme patience during the past two years.*

## Table of Contents

Title .....	i
Declaration of Original Work .....	ii
Copyright .....	iii
Advisory Committee .....	iv
Approval of the Master Thesis .....	v
Abstract .....	vii
Title and Abstract (in Arabic) .....	viii
Acknowledgements .....	ix
Dedication .....	x
Table of Contents .....	xi
List of Tables.....	xiii
List of Figures .....	xiv
List of Abbreviations.....	xvi
Chapter 1: Introduction .....	1
1.1 Overview .....	1
1.2 Properties of Molybdenum Disulfide.....	3
1.3 MoS <sub>2</sub> Preparation .....	5
1.3.1 Exfoliation .....	6
1.3.2 Chemical Vapor Deposition (CVD) Synthesis.....	7
1.4 Applications of Molybdenum Disulfide.....	10
1.4.1 Lubricant Applications .....	10
1.4.2 2D Van der Waals Heterostructures .....	11
Chapter 2: Density Functional Theory (DFT).....	12
2.1 Introduction .....	12
2.2 Born-Oppenheimer Approximation .....	13
2.3 The Hartree Approximation .....	14
2.4 The Hartree-Fock Approximation.....	18
2.5 The Hohenberg-Kohn Theorems.....	18
2.6 The Kohn-Sham equations .....	22
2.7 The Exchange-Correlation Approximations .....	23
2.8 The Linearized Augmented Plane Wave Method .....	24
2.9 Computation on Solids: Electronic Band Structure. ....	26
2.10 Density of States .....	30
Chapter 3: Exchange Correlation Potential.....	34
3.1 The Generalized Gradient Approximation.....	34

3.1.1 Introduction .....	34
3.1.2 Theory .....	35
3.2 Modified Becke-Johnson Scheme.....	39
3.2.1 Introduction .....	39
3.2.2 Theory .....	40
3.3 LDA+U .....	43
3.4 Hybrid Functional .....	46
Chapter 4: Methodology .....	49
4.1 WIEN2k Package .....	49
4.2 VASP .....	52
Chapter 5: Results and Discussion.....	55
5.1 Optimization.....	55
5.2 Electronic Structure Calculations.....	57
5.2.1 Bulk MoS <sub>2</sub> Calculations .....	57
5.2.2 Monolayer MoS <sub>2</sub> Calculations .....	63
5.2.3 Partial Density of States .....	66
5.3 Effect of Interstitial Substitution and Heterostructure on the Electronic Properties.....	68
5.4 Effect of Pressure on the Electronic Properties.....	73
Chapter 6: Conclusion.....	79
References .....	80

## List of Tables

Table 1: Atomization energy of some molecules in Kcal/mol ( 1eV = 23.06 Kcal/mol) using different approximations.....	38
Table 2: Bond length in Bohr for some molecules using different approximations ..	39
Table 3: The value of the band gaps for several solids using different approximations along with the value of c calculated using equation (73) .....	42
Table 4: Band gap calculations for 3-d transition metal monoxides.....	46
Table 5: Band gaps in [eV] for four semiconductors with three different numerical approximations and experimental results .....	48
Table 6: The parameters used to build the molybdenum disulfide structure .....	50
Table 7: The lattice parameters (a,b and c) using WIEN2k and VASP with the mean absolute error .....	56
Table 8: The band gap of the bulk MoS <sub>2</sub> using different approximations implemented in both VASP and WIEN2k package .....	59
Table 9: Band gap and fermi energy level for monolayer MoS <sub>2</sub> using different approximations .....	63
Table 10: Induced band gap reduction with increasing pressure. Pressure, Volume, lattice parameters and Band gap were calculated.....	75

## List of Figures

Figure 1: Bulk MoS <sub>2</sub> imaging a) An image of the bulk MoS <sub>2</sub> b) a Close-up SEM image of MoS <sub>2</sub> nano-flakes from noncentrifuged MoS <sub>2</sub> dispersion .....	3
Figure 2: Three-dimensional representation of the structure of MoS <sub>2</sub> . The intralayer distance between two Mo atoms is 6.55 Å .....	4
Figure 3: CVD preparation of MoS <sub>2</sub> a) sulfurization of MoO <sub>3</sub> b) sulfurization of Mo films c) thermal decomposition of (NH <sub>4</sub> ) <sub>2</sub> MoS <sub>4</sub> .....	9
Figure 4: A system of two hydrogen atoms where A & B denote the nuclei and 1&2 denote the electrons .....	13
Figure 5: Division of the unit cell into two regions 1) the atomic spheres and 2) the interstitial region.....	25
Figure 6: The E(K) relation for an S orbital, K in the range [0,2πa <sub>0</sub> ] with a band width of 4γ .....	29
Figure 7: Electron in a box of length L. With V(x,y,z) = 0 inside the box and ∞ outside.....	30
Figure 8: Two-dimensional array of allowed quantum states represented by the dots.	31
Figure 9: Positive octant part of the sphere for K <sub>x</sub> , K <sub>y</sub> , K <sub>z</sub> > 0 .....	32
Figure 10: Schematic figure of the band gap a) The overlap between the valence and the conduction band with an overlap width W for metals. b) Shows the prevailing of the electrons coulomb repulsion on their Kinetic energy .....	43
Figure 11: The decay properties of the screened coulomb potential (SR-HF) and the Hartree Fock potential. SR-HF decays exponentially with distance from center cell for carbon nanotube .....	47
Figure 12: The crystal structure of a) Monolayer MoS <sub>2</sub> b) Bulk MoS <sub>2</sub> , the hexagonal lattice is clear .....	51
Figure 13: Interstitial substitution crystallography a) Hydrogen atom substitution in Sulfur vacancy b) Nitrogen substitution in Sulfur vacancy c) Boron substitution in Sulfur vacancy .....	52
Figure 14: MoS <sub>2</sub> - WSe <sub>2</sub> Heterostructure.....	54
Figure 15: Optimization a) Energy in Rydberg [Ry] versus c/a % using WIEN2k to find the optimized lattice constants b) Energy versus volume using VASP to find the optimized volume and lattice constants.....	55
Figure 16: Energy versus K-mesh points to find the optimized k-mesh. K mesh saturates at 3×3×1.....	56
Figure 17: Electron Density around MoS <sub>2</sub> along the plane (110) .....	57
Figure 18: The band structure (left) and DOS (right) of bulk MoS <sub>2</sub> using a) GGA b) MBJ .....	60

Figure 19: The band structure (left) and DOS (right) of bulk MoS <sub>2</sub> using a) LDA+U b) On Site Hybrid functional .....	61
Figure 20: The band structure (left) and DOS (right) of bulk MoS <sub>2</sub> using a) GGA b) LDA+U c) on-site hybrid functional implemented in VASP which shows an indirect band gap.....	62
Figure 21: The band structure (left) and DOS (right) of monolayer MoS <sub>2</sub> using a) GGA b) LDA+U c) onsite Hybrid functional implemented in WIEN2k, which shows a direct band gap .....	64
Figure 22: The band structure (left) and DOS (right) of monolayer MoS <sub>2</sub> using a) GGA b) LDA+U using VASP, which shows a direct band gap .....	65
Figure 23: Partial density of states for the molybdenum atom and its s and d orbitals using a) GGA08 b) GGA+U c) onsite hybrid functional d) MBJ.....	66
Figure 24: Partial density of states for the Sulfur atom and its s and p orbitals using a) GGA08 b) GGA+U c) onsite hybrid functional d) MBJ .....	67
Figure 25: Band structure of ML MoS <sub>2</sub> with B substitution in Sulfur vacancy using a) GGA b) up spin channel c) down spin channel .....	70
Figure 26: Band structure of ML MoS <sub>2</sub> with Hydrogen substitution in Sulfur vacancy using a) GGA b) up spin channel c) down spin channel .....	71
Figure 27: Band structure of monolayer MoS <sub>2</sub> with Nitrogen substitution in Sulfur vacancy .....	72
Figure 28: The band structure of MoS <sub>2</sub> -WSe <sub>2</sub> using LDA+U.....	72
Figure 29: Behavior of the volume with respect to pressure.....	74
Figure 30: Behavior of the band gap with respect to pressure (While pressure increases the band gap decreases) .....	74
Figure 31: Effect of negative pressure a) The band structure of MoS <sub>2</sub> under negative pressure b) DOS of MoS <sub>2</sub> under negative pressure. ....	76
Figure 32: The band structure of MoS <sub>2</sub> under positive pressure. The arrows show the direction of increasing pressure .....	77
Figure 33: DOS of MoS <sub>2</sub> under positive pressure. ....	78



## List of Abbreviations

2D	Two-Dimensional
CVD	Chemical Vapor Deposition
DFT	Density Functional Theory
DOS	Density of States
eV	Electron Volt (energy unit)
FET	Field Effect Transistor
GGA	Generalized Gradient Approximation
H-F	Hartree-Fock Approximation
H-K	Hohenberg-Kohn Theorems
K-S	Kohn-Sham Equation
LAPW	Linearized Augmented Plane Wave
LDA	Local Density Approximation
LDA+U	Local Density Approximation+ Hubbard energy U
LMTO's	Linearized Muffin Tin Orbitals
LO	Local Orbitals
LSD	Local Spin Density Approximation
MAE	Mean Absolute Error

MBJ	Modified Becke-Johnson Approximation
PAW	Projector Augmented Wave
PBE	Perdew- Burke- Ernzerhof GGA Approximation
PW91	Perdew-Wang 1991 GGA Approximation
TMDC's	Transition Metal Dichalcogenides
VASP	Vienna Ab-initio Simulation Package
XC	Exchange Correlation Potential Energy

## Chapter 1: Introduction

### 1.1 Overview

The interest in 2-dimensional (2D) semiconductors is largely fueled by the highly successful miniaturization of Si-based electronic devices for higher packing density, faster circuit speed, and lower power dissipation.

The bulk form of many layered materials were found long time ago and they were used as dry lubricant such as graphite and Molybdenum disulfide  $\text{MoS}_2$  due to their layered nature. Atoms are strongly attracted to each other within the same plane by a strong covalent or ionic bonding but the interlayer attraction is due to a weak Van der Waals force, which makes it easy to extract one or few layers of the material.

2D Materials consist of a range of distinct electronic properties. Some are semiconductors with a big direct band gap (5.8 eV) like boron nitride [1], transition metal dichalcogenides (TMDCs) such as molybdenum disulfide ( $\text{MoS}_2$ ) -which we will be studying – and tungsten diselenide ( $\text{WSe}_2$ ). Others are semi-metallic such as the promising 2D graphene (single layer of graphite).

Comparing layered materials to the known - and widely used- photonic materials such as gallium arsenide (GaAs) or silicon (Si) one may find that the layered material may be a very good alternative in electronic and photonic devices. Since the 2D materials have a passivated surface<sup>1</sup> that makes it easy to create heterostructures using two different 2D materials (say for example  $\text{MoS}_2$  –  $\text{WSe}_2$  heterostructure) without any problem of lattice mismatch issue since they will be attracted by Van der Waals forces just like their bulk sheets do. Many 2D materials interact with light very

---

<sup>1</sup> There are no dangling bonds on the surface so it will not interact with the surrounding environment

strongly and they may cover a long range of the electromagnetic spectrum, for example, the semi metallic graphene interacts with the electromagnetic spectrum from the range of the microwave to the ultraviolet region which makes it a very good material for light detection applications [2].

The recently discovered 2D materials have gained the researchers interest for its promising applications in the optical and electrical industries. Graphene, with its high optical transparency (97.7% transmittance in the visible spectrum), good thermal conductivity at room temperature ( $3 \times 10^3$  W/mK) and exceptional mechanical strength (Young's modulus of 1.1TPa) opened new era in the technologies of photonics and optoelectronics. These properties put graphene in the top of the list as a candidate for transparent electrodes, energy storage and solar cells industries. These outstanding characterizations enhanced the demand to search more in the field of 2D layered materials. One major disadvantage in graphene is that it lacks the existence of a band gap therefore it is not considered as an optimal material for light emission devices and it minimized its application in the electronic industry where semiconductor materials maybe of much use. On the contrary, single layer TMDCs such as MoS<sub>2</sub> are considered as direct band gap semiconductors and they exhibit good light emitting properties [2].

The main goal of this work is to contribute toward an accurate theoretical determination of the electronic properties of a monolayer and multilayer MoS<sub>2</sub>. We plan to investigate the effect of pressure on the band gap energies and the density of states of MoS<sub>2</sub>.

## 1.2 Properties of Molybdenum Disulfide

Molybdenum disulfide ( $\text{MoS}_2$ ) is one of the 2D material, which offers a great promise for device applications especially in the optoelectronics and energy harvesting which requires thin semiconductors; it can also be used along with graphene where both materials may complement each other.  $\text{MoS}_2$  has gained a lot of interest for its properties, which differs if you deal with the 2D monolayer or with its 3D bulk form. It was widely used as a solid lubricant since its first discovery in 1960 [3].

$\text{MoS}_2$  is a black / grey material (figure 1) similar to Graphite with a molar mass of  $160.07 \text{ g/mole}$  and a density of  $5.06 \text{ g/cm}^3$ . It has a very high melting point just like the other layered materials that may exceed  $1000^\circ \text{C}$  and is insoluble in water. It has a 2H hexagonal structure with space group  $\text{P6}_3/\text{mmc}$  [5].

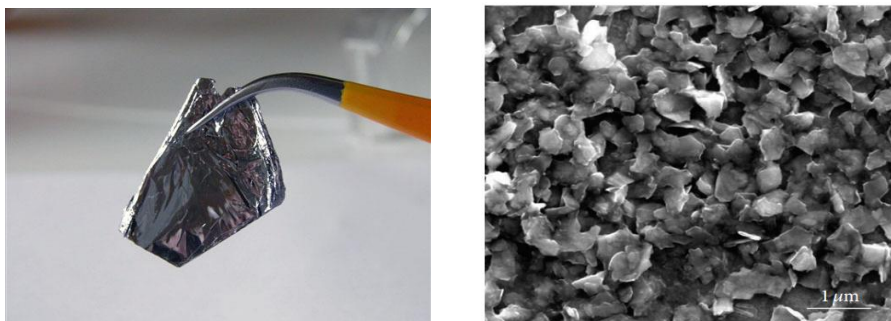


Figure 1: Bulk  $\text{MoS}_2$  imaging a) An image of the bulk  $\text{MoS}_2$  b) a Close-up SEM image of  $\text{MoS}_2$  nano-flakes from noncentrifuged  $\text{MoS}_2$  dispersion [4]

The  $\text{MoS}_2$  crystal consists of layers attracted by Van der Waals force, which explains the ease to exfoliate few layers or even one layer from the bulk form. Each layer is built of a sheet of Molybdenum ( $\text{Mo}^{+4}$ ) sandwiched between two sheets of Sulfur ( $\text{S}^{-2}$ ) as shown in (figure 2). Depending on the arrangement of S atoms, the 2D monolayer  $\text{MoS}_2$  may appear in two different symmetries that may affect its electronic

structure and properties. The first is 2H, which is trigonal prismatic, acquires semiconducting properties. The other form is the metallic 1T, which is Octahedral  $O_h$  phase. Yung-Chang *et.al* have showed that the transition between these two phases is possible by intra-layer atomic plane glide [6].

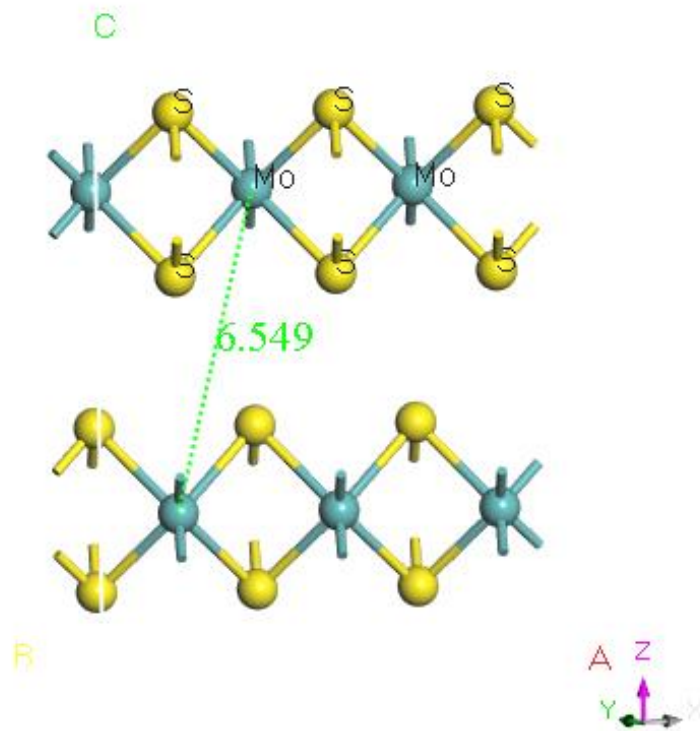


Figure 2: Three-dimensional representation of the structure of  $\text{MoS}_2$ . The inter-layer distance between two Mo atoms is  $6.55 \text{ \AA}$

Similar to graphene,  $\text{MoS}_2$  has a Young's modulus of  $033 \pm 0.07 \text{ TPa}$  which makes it mechanically flexible [7].

During the early 2010, Raman Changgu Lee's group ran spectra characterization on a single and few layers of  $\text{MoS}_2$ . They aimed to investigate two peaks  $E_{2g}^1$  and  $A_{1g}$  to reflect the crystal structure of  $\text{MoS}_2$ .  $E_{2g}^1$  In addition,  $A_{1g}$  are indicators of in-plane and out-of-plane vibrational modes of S atoms respectively. From bulk to monolayer, three changing parameters are collected, first,  $E_{2g}^1$  exhibits a

blue shift whereas the  $A_{1g}$  undergoes a red shift. The second note is the difference of frequency between the two peaks reduces proportionally with respect to the number of layers where it ranges from  $25\text{ cm}^{-1}$  in the bulk characterization to  $19\text{ cm}^{-1}$  for the monolayer  $\text{MoS}_2$ . The third note is that the intensities of the peaks increases linearly with increasing the layer thickness up to four layers [8].

The thermal conductivity of few layers of  $\text{MoS}_2$  was estimated to be  $52\text{ W/mK}$  [9]. Opposing the graphene that is highly sensitive to light but has low photo response,  $\text{MoS}_2$  has a high photo response.

$\text{MoS}_2$  exhibits good electrical and transport properties, and is chemically and thermally stable, transparent, flexible, and relatively inexpensive, which all together makes this material an excellent candidate for a variety of electronic and optoelectronic applications. The 2D form of the material was not discovered until 2011 when scientists succeeded in producing a transistor made from this new material.

Molybdenum disulfide looks to be a promising class of material for next-generation electronics, as it is the only 2D material yet discovered which has an inherent band gap. With this feature, molybdenum disulfide paves the way for the development of a very new domain of electronic devices and materials, which can be used in heterostructures with other 2D layered materials to complement each other.

### **1.3 $\text{MoS}_2$ Preparation**

This work will not involve any experimental preparation but I must say that this material (few layers or single layer  $\text{MoS}_2$ ) can be prepared experimentally. The preparation techniques may vary from exfoliation to Chemical vapor decomposition.

### 1.3.1 Exfoliation

Exfoliating graphene from graphite successfully opened the door to use this technique on other graphene-like two-dimensional materials such as MoS<sub>2</sub>. Though this method is useful for fundamental research, it cannot be used for large-scale applications because of the inaccuracy in defining the number of layers.

Karim *et al.* used a technique called anodic bonding to fabricate a two-dimensional few layers of MoS<sub>2</sub>. Anodic bonding is a process used to seal glass to either silicon or a metal without any intermediate layer by different techniques such as sputtering. Hua Zhang *et al.* used exfoliation based on chemical reactions through an electrochemical lithium discharge process. After several ultra-sonication, they were able to achieve a 92% high yield monolayer MoS<sub>2</sub>.

The last exfoliation technique to present in this thesis is the approach used by O'Neill *et al.* They exfoliated bulk MoS<sub>2</sub> by suspending it in an organic solvent. They were able to control the sonication time, which improved the efficiency of this approach to produce a higher concentration of flakes (up to 40 mg/mL). Chemical exfoliation seems to be more productive with a disadvantage of creating more defects in the structure of the two-dimensional layered materials. The defects in structure due to the sonication may affect the flakes size and constrict the produced 2D material applications in the large-scale integrated circuits [10].



### 1.3.2 Chemical Vapor Deposition (CVD) Synthesis

CVD is a technique used for material processing. During CVD, a precursor<sup>2</sup> is being delivered to a reaction chamber where it passes over a heated substrate under a critical temperature that is required for a specific reaction to take place after the precursor is diffused on the surface. In addition, the required products will be adsorbed in the substrate with the by-product being desorbed and removed from the chamber. At the end, you will get the substrate coated by the desired material.

This technique is very useful in preparing 2D layered materials and their heterostructure since it allows to control the thickness of your sample. CVD is a better choice than transporting layer by layer for creating a heterostructure because of its advantages in reducing the interfacial contamination. Since synthesizing 2D layered materials on a wafer scale using CVD is possible, it will give the industry the potential to use the produced materials in large-scale application.

Using this technique in preparing MoS<sub>2</sub> is possible using different kinds of precursors such as Mo based compounds, (NH<sub>4</sub>)<sub>2</sub>MoS<sub>4</sub> and graphene /MoS<sub>2</sub> composites.

#### 1.3.2.1 Sulfurization of Mo based compound and Mo based Oxides

In 2012, Lain-Jong Li *et al.* used Molybdenum trioxide (MoO<sub>3</sub>) and Sulfur powder (S) as solid reactants to synthesis large-scale monolayer MoS<sub>2</sub> films on a silicon dioxide (SiO<sub>2</sub>) coated by graphene substrate. The field effect transistors (FET)

---

<sup>2</sup> Precursors are the compounds used in chemical reactions to produce other compounds.

produced from this film have an on/off ratio of  $10^4$  with an n-type behavior (Figure 3.a).

One year later, Yifei Yu *et al.* demonstrated that the replacement of  $\text{MoO}_3$  by molybdenum chloride ( $\text{MoCl}_5$ ) might improve the performance of the FET with a mobility that could reach up to  $0.03 \text{ cm}^2/\text{V}\cdot\text{s}$ .

Yongie Zhan *et al.* used a different approach where they pre-deposited Mo thin layer on a  $\text{SiO}_2$  substrate using electron beam physical vapor deposition. The substrate would then be placed in furnace at  $750^\circ \text{C}$  to react with sulfur vapor. The result samples were bi-layers and tri-layers with typical mobility in the range  $0.004 - 0.04 \text{ cm}^2/\text{V}\cdot\text{s}$  (Figure 3. b) [11].

#### **1.3.2.2 Thermal decomposition of $(\text{NH}_4)_2\text{MoS}_4$**

$\text{MoS}_2$  films created using Thermal decomposition of  $(\text{NH}_4)_2\text{MoS}_4$  showed an excellent bottom gated FE electron mobility that reached  $4.7 \text{ cm}^2/\text{V}\cdot\text{s}$ . Keng Ku Liu *et al.* were able to fabricate a bi layer and a tri layer films on an insulating substrate. This approach should be done with extreme caution to achieve homogeneous precursor films on target substrate (Figure 3.c) [11].

#### **1.3.2.3 Direct synthesis of graphene/ $\text{MoS}_2$ composites**

Creating heterostructures from the 2D layered materials is of a great concern in the optoelectronics and electronic industry. Since the graphene was the first 2D material to be examined and showed promising features with some limitations in specific applications (graphene is a gapless material) it would highly be interesting to study its features in heterostructures with other 2D materials.

Layer by layer stacking has been the simplest way of creating the heterostructures with the disadvantage of interfacial contamination. So far the substrates used for preparing MoS<sub>2</sub> were mainly SiO<sub>2</sub>, Mica or sapphire, but it was shown that graphene itself might be used as a substrate for growing MoS<sub>2</sub>. Yumen Shi *et al.* showed that hexagonal MoS<sub>2</sub> nano-flakes with a crystal size ranging from hundred nanometers to few micrometers were deposited on top of a graphene layer with a small lattice mismatch. Recently (In 2014), Kathleen M. *et al.* reported growing a uniform monolayer MoS<sub>2</sub> on a large area graphene with a heterostructure size up to centimeters which is more controllable and practical. Being able to create such heterostructure will allow us to use the features of both materials simultaneously [11].

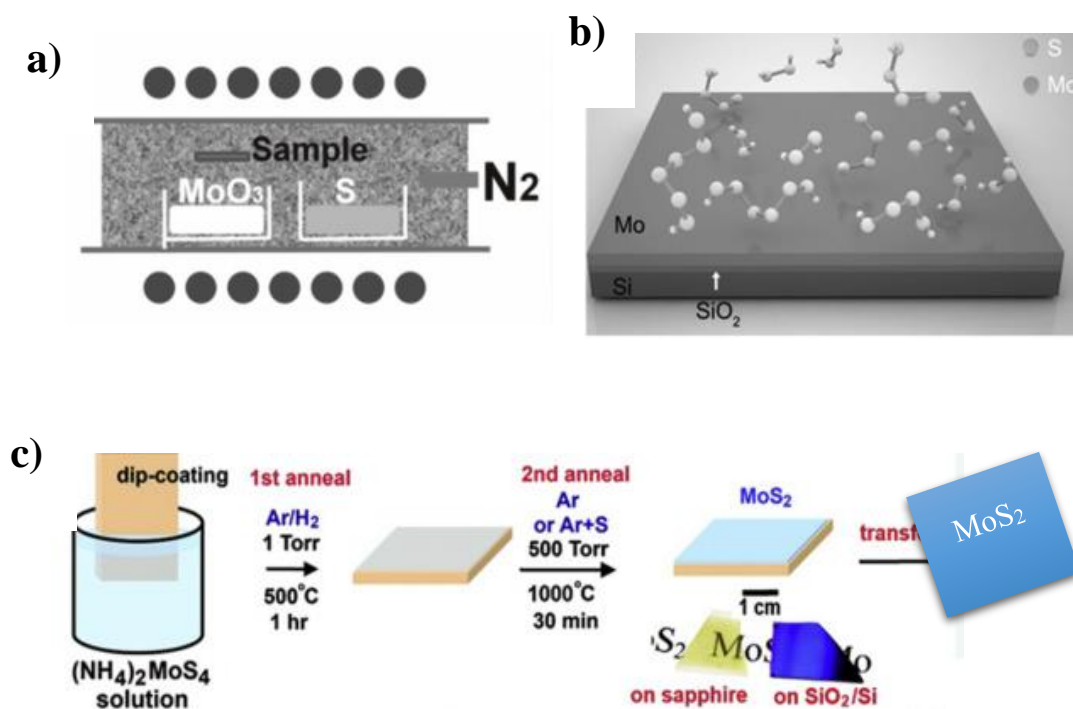


Figure 3: CVD preparation of MoS<sub>2</sub> a) sulfurization of MoO<sub>3</sub> b) sulfurization of Mo films c) thermal decomposition of (NH<sub>4</sub>)<sub>2</sub>MoS<sub>4</sub>

## 1.4 Applications of Molybdenum Disulfide

MoS<sub>2</sub>, just like graphene, has various applications in many fields as a bulk and in its monolayer form. Due to its optical and electrical characterizations, and since it is the most abundant TMDCs, it expanded into a wide researched topic to be used in related applications.

### 1.4.1 Lubricant Applications

Lubricants are materials used to protect other materials and surfaces from being damaged due to friction or wear. Lubricants are usually liquids or gases, but solids have an excellent feature in providing lubricant features as solid lubricants or dry lubricant. For the solid to work as a lubricant, it must acquire some preferred properties. First, it must be able to maintain a low and controlled friction between the surfaces. It should be chemically stable under a range of specified temperatures that are required for the designed application and adhere strongly to one of the surfaces, so that it does not get lost rapidly. Finally, yet importantly, it must be non-toxic with sufficient wear resistance.

Shankara. A *et al.* have tested phosphate steel specimens coated by MoS<sub>2</sub> while applying a scratch test. They found that the average wear rate was 0.215  $\mu\text{m}/\text{cycle}$  and the initial coefficient of friction around 0.08. They also studied the addition of 8% zirconia and 25% graphite on MoS<sub>2</sub> and they found that the wear resistance increased to reach 0.003  $\mu\text{m}/\text{cycle}$  and the initial coefficient of friction 0.06 [3].

### 1.4.2 2D Van der Waals Heterostructures

MoS<sub>2</sub> gained the researchers interest since it is one of the most abundant TMDCs. It can be used in many applications such as transistors, photo detectors, solar cells, Lubricant applications, etc. However, due to its intrinsic properties, it has some limitations that constrict its applications in some applications. For example, MoS<sub>2</sub> electron mobility is much less than graphene which makes it a bad candidate to act as transparent electrodes. Graphene on the other hand, shows a great mobility with outstanding electrical performance but since it has a zero band gap it fails in the switch control applications.

An excellent alternative to using these two materials separately is to use a hybrid heterostructure employing the controllable band gap of MoS<sub>2</sub> to enhance the performance of the gapless graphene.

In 2011, Yandong Ma *et al.* calculated the binding energy of carbon (C) atom to MoS<sub>2</sub> to be 23 eV with an interlayer spacing between graphene and MoS<sub>2</sub> to be 3.32 Å. This structure introduced a 2 meV band gap of graphene, which is almost negligible but may be tuned by varying the interlayer spacing [12].

Marco.B *et al.* have shown that a type 2 Schottky junction (MoS<sub>2</sub>/graphene) of 0.9 nm thickness exhibit a high power conversion efficiency that may reach 1% and power density of 0.25 – 2.5 mW/Kg which is higher than the known ultrathin solar cells (GaAs and Si) by 1- 3 order of magnitudes [13].

## Chapter 2: Density Functional Theory (DFT)

### 2.1 Introduction

Solid state physics deals with studying the rigid materials, their crystallography, the electromagnetism and the electronic structure. The simplest form of any material is its unit cell. The unit cell may contain different atoms (many electrons) at different positions, which is repeated periodically to form a crystal.

Quantum mechanics gives us the opportunity to study the electronic structure of any material, and helps us to understand many other properties such as phase transition, relative stability and electrical, mechanical, optical or magnetic properties. With a huge number, such as the Avogadro's number of atoms, the problem in Quantum mechanics becomes very complicated to solve manually.

One of the basic problems in theoretical physics and chemistry is the description of the structure and dynamics of many-electrons systems. The Density Functional Theory (DFT) is a modeling method to study the electronic structure calculations, which ranks among the most computationally intensive tasks in all scientific calculations. This method helps to deal with problem of  $N$ -particle (electrons) in 3-spatial coordinates as a problem of one main variable which is the electron density [14].

Density functional theory uses several approximations, which we will describe in the following sections.

## 2.2 Born-Oppenheimer Approximation

We will consider a system of two hydrogen atoms with two nuclei A and B and two electrons 1 and 2 as shown in figure 4.

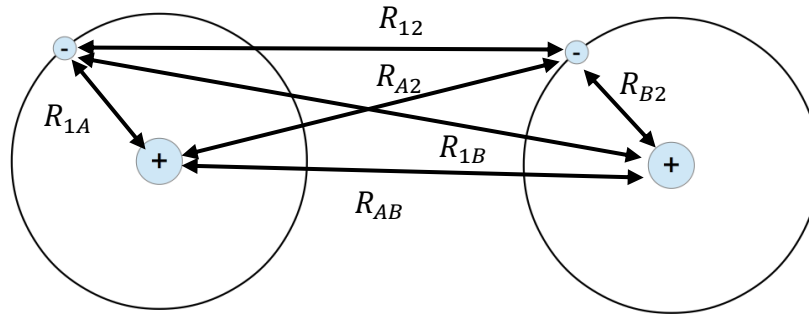


Figure 4: A system of two hydrogen atoms where A & B denote the nuclei and 1&2 denote the electrons

The general molecular Schrödinger equation, apart from electron spin effects, is

$$\hat{H}\psi = E\psi, \quad (1)$$

where  $H$  is the Hamiltonian operator and  $E$  is the energy eigenvalue.

Considering the kinetic energy of each electron and nuclei in the system described above and the electric potential energy for all possible interactions, the Hamiltonian of the system is [15]:

$$\begin{aligned} \hat{H} &= \hat{T} + \hat{V} \\ \hat{H} &= -\frac{\hbar^2}{2m} \hat{\nabla}_A^2 - \frac{\hbar^2}{2m} \hat{\nabla}_B^2 - \frac{\hbar^2}{2m} \hat{\nabla}_1^2 - \frac{\hbar^2}{2m} \hat{\nabla}_2^2 \\ &\quad + \frac{e^2}{4\pi\epsilon_0} \left( \frac{1}{R_{12}} - \frac{1}{R_{1A}} - \frac{1}{R_{A2}} - \frac{1}{R_{1B}} - \frac{1}{R_{B2}} + \frac{1}{R_{AB}} \right) \end{aligned} \quad (2)$$

where  $T = -\frac{\hbar^2}{2m} \nabla_i^2$  is the Kinetic energy operator of electron  $i$  and  $V = \frac{e^2}{4\pi\epsilon_0} \frac{1}{R_{ij}}$  is the potential energy between objects  $i$  and  $j$ .

Since the nuclear mass is much greater than the electron mass, the Born Oppenheimer approximation, which is the first approximation used in DFT, defines the nuclear position as being fixed so that the kinetic energy of the nucleus will equal to zero compared to the kinetic energy of the electron.

Then, the electronic Hamiltonian can be rewritten as:

$$\hat{H}_{elc} = -\frac{\hbar^2}{2m} \nabla_1^2 - \frac{\hbar^2}{2m} \nabla_2^2 + \frac{e^2}{4\pi\epsilon_0} \left( \frac{1}{R_{12}} - \frac{1}{R_{1A}} - \frac{1}{R_{A2}} - \frac{1}{R_{1B}} - \frac{1}{R_{B2}} + \frac{1}{R_{AB}} \right), \quad (3)$$

where  $\frac{1}{4\pi\epsilon_0} \frac{e^2}{R_{AB}}$  is considered as a constant which we will consider later as the external potential

### 2.3 The Hartree Approximation

Hartree approximation uses the same concept that is used in variational method. The Hartree approximation starts with a guess of the wave function and just run a self-consistent cycle until we reach convergence but we will come to that later in more details. The Hartree approximation does not follow Pauli Exclusion Principle since it does not take the antisymmetry due to interchange of coordination into account, so correlation due to Pauli principles are ignored but one should ensure that no two electrons are occupying the same state.

Hartree theory starts with defining the wave function by equation (4).

$$\psi(X) = \prod_{i=1}^N \phi_i(x) \quad (4)$$



where  $\phi_i(\mathbf{x}) = \psi_i(\mathbf{r})\chi_i(\sigma)$ .

The Schrödinger differential equation of the system is now defined as:

$$\left[-\frac{1}{2}\nabla^2 + v(\mathbf{r}) + v_{ee}^H(\mathbf{r})\right]\phi_i(\mathbf{x}) = \epsilon_i\phi_i(\mathbf{x}) \quad i = 1, \dots, N \quad (5)$$

where  $v_{ee}^H(\mathbf{r})$  is the local effective electron- interaction potential energy.

$v(\mathbf{r})$  is the external potential energy.

$v_{ee}^H(\mathbf{r})$  is defined as the work required to move the model fermion (electrons) due to the force of the conservative field, the effective Hartree field  $\mathcal{F}^H(\mathbf{r}')$ .

$$v_{ee}^H(\mathbf{r}) = -\int_{\infty}^{\mathbf{r}} \mathcal{F}^H(\mathbf{r}') \cdot d\mathbf{l}' \quad (6)$$

Where  $\mathcal{F}^H(\mathbf{r}')$  is the summation of the electron interaction field  $\epsilon_{ee}^H(\mathbf{r})$  and the correlation kinetic field  $Z_{tc}^H(\mathbf{r})$ .

$$\mathcal{F}^H(\mathbf{r}') = \epsilon_{ee}^H(\mathbf{r}') + Z_{tc}^H(\mathbf{r}') \quad (7)$$

With  $\nabla \times \mathcal{F}^H(\mathbf{r}') = 0$  so that  $v_{ee}^H(\mathbf{r})$  is path independent.

The term  $\epsilon_{ee}^H(\mathbf{r})$  is obtained from the hartree pair correlation density  $g^H(\mathbf{r}\mathbf{r}')$  via coulomb law.

$$\epsilon_{ee}^H(\mathbf{r}) = \int \frac{g^H(\mathbf{r}\mathbf{r}')}{|\mathbf{r}-\mathbf{r}'|^3} d\mathbf{r}' \quad (8)$$

The Hartree pair correlation density is a property representing the electrons correlation due to Pauli principles or coulomb interactions and is defined mathematically as:

$$g^H(\mathbf{r}\mathbf{r}') = \frac{P(\mathbf{r}\mathbf{r}')}{\rho(\mathbf{r})} \quad (9)$$

Where  $\rho(\mathbf{r})$  is the electronic density and  $P(\mathbf{r}\mathbf{r}')$  is the expectation value of the pair correlation operator  $\hat{P}(\mathbf{r}\mathbf{r}')$  that gives the probability of finding the electron at  $\mathbf{r}$  and  $\mathbf{r}'$  simultaneously. The effect of the pair correlation density is valid and necessary. According to Pauli's exclusion principle, no two electrons can be at the same quantum state and the repulsion due to the Coulomb force will affect the local density of the electrons at  $r'$  and from this concept comes the importance of the pair correlation density. This change in the local density is called the Fermi coulomb hole charge distribution  $\rho_{XC}(\mathbf{r}\mathbf{r}')$ , which is a nonlocal self-interaction correlation (SIC). According to what we said, the pair correlation density can be rewritten as the summation of the local and the nonlocal densities:

$$g^H(\mathbf{r}\mathbf{r}') = \rho^{SIC}(\mathbf{r}\mathbf{r}') + \rho(\mathbf{r}') \quad (10)$$

Now substituting equation (10) in equation (8), we get:

$$\varepsilon_{ee}^H(\mathbf{r}) = \int \frac{\rho^{SIC}(\mathbf{r}\mathbf{r}')(r-r')}{|r-r'|^3} d\mathbf{r}' + \int \frac{\rho(\mathbf{r}')(r-r')}{|r-r'|^3} d\mathbf{r}' \quad (11)$$

$$\varepsilon_{ee}^H(\mathbf{r}) = \varepsilon_H(\mathbf{r}) + \varepsilon_H^{SIC}(\mathbf{r}) \quad (12)$$

Combining equation (12) and equation (7), we get:

$$\mathcal{F}^H(\mathbf{r}') = \mathcal{Z}_{tc}^H(\mathbf{r}) + \varepsilon_H(\mathbf{r}) + \varepsilon_H^{SIC}(\mathbf{r}) \quad (13)$$

In addition, from equation (6) we may find  $v_{ee}^H(\mathbf{r})$  to be:

$$v_{ee}^H(\mathbf{r}) = - \int_{\infty}^r \mathcal{Z}_{tc}^H(\mathbf{r}) + \varepsilon_H(\mathbf{r}) + \varepsilon_H^{SIC}(\mathbf{r}). dl' \quad (14)$$

Choosing the correct symmetry such that all the above fields are conservative, we can simplify equation (14) as:

$$v_{ee}^H(\mathbf{r}) = W_H(\mathbf{r}) + W_H^{SIC}(\mathbf{r}) + W_{tc}^H(\mathbf{r}) \quad (15)$$

where  $W_H(\mathbf{r})$ ,  $W_H^{SIC}(\mathbf{r})$ ,  $W_{tc}^H(\mathbf{r})$  are the separate work done by the fields  $\varepsilon_H(\mathbf{r})$ ,  $\varepsilon_H^{SIC}(\mathbf{r})$ ,  $\mathcal{Z}_{tc}^H(\mathbf{r})$  respectively.

Now applying Schrödinger's equation, we may find that the total energy of Hartree theory written in term of the fields is:

$$E^H = T_s + \int \rho(r)v(r)dr + T_c^H(\mathbf{r}) + E_H(\mathbf{r}) + E_H^{SIC}(\mathbf{r}) \quad (16)$$

Where the first term in Schrodinger equation is due to the Kinetic energy  $\langle \phi_i(\mathbf{r}\sigma) | -\frac{1}{2}\nabla^2 | \phi_i(\mathbf{r}\sigma) \rangle$  and the second term is due to the external field. The third, fourth and fifth terms are due to  $W_{tc}^H(\mathbf{r})$ ,  $W_H(\mathbf{r})$  and  $W_H^{SIC}(\mathbf{r})$  respectively [16].

The difficulty in solving N particle problems is that the potential of each particle is related to the other N-1 particles. That is why this method is self-consistent and one may solve it by finding  $\phi_i(x)$  that may be a solution to the Hartree equation. The following steps will summarize the approach:

First: GUESS a set of one-particle states  $\phi_i(x)$ .

Second: Using the guessed state, Find  $V_H(\mathbf{r})$ .

Third: Solve the one particle Hartree equation using  $V_H(\mathbf{r})$ .

Fourth: If the found states are the same as the guessed states then we are done, if not, then use the new states as guessed ones and repeat from the first step until you reach convergence. To avoid any oscillations, it is better for the new guessed state to be a mixture of the old guessed state and the last solution obtained from step four [17].

## 2.4 The Hartree-Fock Approximation

The Hartree approximation is considered as a good introduction to the methods of solving the many particles systems. In fact, the Hartree approximation is not perfectly correct and it is safe to say that it is wrong since the wave functions are not antisymmetric.

The Hartree-Fock (H-F) approximation follows the same procedure used in the Hartree approximation but by taking the antisymmetric wave function as a requirement. To do so, H-F approximation uses a Slater determinant to define the wave function.

$$\psi = \frac{1}{\sqrt{N!}} \sum_{(n_1, n_2, \dots)} \epsilon_{n_1 n_2 \dots} \psi_{n_1}(\mathbf{r}_1) \psi_{n_2}(\mathbf{r}_2) \dots \quad (17)$$

Note that; the indices indicate the single particle state and not the particle coordinates [18], [19].

The wave function can also be written as;

$$\psi(1, \dots, N) = \frac{1}{\sqrt{N!}} \det \begin{bmatrix} \psi_1(\mathbf{1}) & \dots & \psi_1(\mathbf{N}) \\ \vdots & \ddots & \vdots \\ \psi_N(\mathbf{1}) & \dots & \psi_N(\mathbf{N}) \end{bmatrix} \quad (18)$$

According to the properties of the determinant, the exchange of two columns - that corresponds to exchanging two particles- will result on a minus sign. Moreover, if two rows are the same, then the determinant will be zero, which demonstrates Pauli's exclusion principle. Then we may apply the same procedure used in section 2.3.

## 2.5 The Hohenberg-Kohn Theorems

As we discussed earlier in section 2.2, the Born-Oppenheimer approximation freezes the nuclei since they are much heavier and therefore much slower than the

electrons. In other words, only the electrons are kept as players in our many body problem. The nuclei are treated as a source of positive charge; they become ‘external’ to the electron cloud. After applying this approximation, we are left with a much simpler Schrödinger equation:

$$\hat{H}\psi = [\hat{T} + \hat{U} + \hat{V}]\psi$$

$$\hat{H}\psi = \sum_{i=1}^N \left( -\frac{\hbar^2}{2m_i} \hat{\nabla}^2 \right) + \sum_{i=1}^N \hat{V}(\mathbf{r}_i) + \sum_{i<j}^N \hat{U}(\mathbf{r}_i, \mathbf{r}_j) ] = E\psi \quad (19)$$

Where  $H$  is the Hamiltonian,

$E$  is the energy,

$T$  is the kinetic energy of the particle (electron) " $i$ " ,

$V$  is the external field potential energy due to a positively charge nuclei,

And  $U$  is the  $e^- - e^-$  interaction energy (since electrons are fermions, no two electrons of the same quantum number are allowed to stay in the same energy state) [20].

There are many sophisticated methods to solve the many-particle Schrödinger equation. In DFT, the key variable is the particle (electron) density  $\rho(\mathbf{r})$ . Vice versa, if we have the wave function of the ground state  $\psi_0(r_1, r_2, \dots)$  we will be able to find  $\rho_0(r)$ , which means that  $\psi$  is unique – as said above – . Then, we can say that the expectation value of the Hamiltonian (the energy) is a function of  $\rho_0$ .

$$E_o = E(n_o) = \langle \psi(n_o) | \hat{T} + \hat{V} + \hat{U} | \psi(n_o) \rangle$$

$T$  and  $U$  are universal operators – independent of the system – whereas  $V$  is a non-universal one; and hence the contribution of the external potential  $V$ ,  $\langle \psi(n_o) | V | \psi(n_o) \rangle$ , can be written explicitly in terms of the ground state density  $n_o$

$$V[n_o] = \int V(r) \rho_o(\mathbf{r}) d^3r ; \quad (20)$$

The above remark was stated by the Hohenberg-Kohn theorems (H- K theorems). The H-K theorems were held only for non-degenerate states neglecting any magnetic field. However, they have been improved to encompass these cases. I will only consider the non-degenerate H-K theorems.

The first and second of (H-K) theorems suggests that the ground state of a many-electron systems can be uniquely described by the ground state- electron density as a function of the 3 spatial coordinates only that if approximated correctly, we will be able to find our wave function that minimizes the energy. Therefore, instead of having a problem with N-particle (electrons) in 3-spatial coordinates, we will have a problem of one (electron density) in the 3- spatial coordinates. The (H- K) theorems suggests that there is a one-to-one correspondence between the ground-state density  $n(\mathbf{r})$  of a many-electron system (atom, molecule, solid) and the external potential. This theorem can be proved by assuming two different systems A and B with two different external potentials,  $V_a$  and  $V_b$ , having the same density of state. The two potentials  $V_a$  and  $V_b$  corresponds to two different Hamiltonians  $H_a$  and  $H_b$  respectively. We know that the ground state eigenvalue  $E_{0,a}$  corresponds to a unique ground state wave function  $\psi_{0,a}$ . Where  $a$  refers to the Hamiltonian for the system A. Applying the Hamiltonian of system A on any other wave function other than  $\psi_{0,a}$  will result an energy eigenvalue greater than  $E_{0,a}$ .

$$E_{0,a} < \langle \psi_{0,b} | H_a | \psi_{0,b} \rangle \quad (21)$$

Where “a” refers to system A and “b” refers to system B.

Now subtracting and adding  $H_b$  to the operators will yield to equation 22;

$$\begin{aligned} E_{0,a} &< \langle \psi_{0,b} | H_a - H_b + H_b | \psi_{0,b} \rangle \\ E_{0,a} &< \langle \psi_{0,b} | H_a - H_b | \psi_{0,b} \rangle + \langle \psi_{0,b} | H_b | \psi_{0,b} \rangle \\ E_{0,a} &< \langle \psi_{0,b} | H_a - H_b | \psi_{0,b} \rangle + E_{0,B} \end{aligned} \quad (22)$$

Since we are assuming that the only difference in A and B is in the external potential Equation 22 maybe written as.

$$E_{0,a} < \langle \psi_{0,b} | V_a - V_b | \psi_{0,b} \rangle + E_{0,B} \quad (23)$$

We can write equation 23 in terms of the ground state density;

$$E_{0,a} < \int [V_a - V_b] \rho_{0(r)} d(r) + E_{0,B} \quad (24)$$

Since a and b are interchangeable indices equation 24 may be written as.

$$E_{0,b} < \int [V_b - V_a] \rho_{0(r)} d(r) + E_{0,a} \quad (25)$$

Adding equation 25 and 24;

$$\begin{aligned} E_{0,a} + E_{0,B} &< \int [V_a - V_b] \rho_{0(r)} d(r) + \int [V_b - V_a] \rho_{0(r)} d(r) + E_{0,B} + E_{0,a} \\ (26) \end{aligned}$$

The integration terms will cancel since  $V_a - V_b = -(V_b - V_a)$  and equation 26 becomes;

$$E_{0,a} + E_{0,B} < E_{0,B} + E_{0,a} \quad (27)$$

This clear contradiction proves that our assumption was not valid and that there is a unique one to one correspondence between the external potentials, the wave functions and the electron density. H-K theorems suggest that there exists a density function (theorem 1) that helps us find the optimized Hamiltonian and wave function in order to find the corresponding minimum eigenvalue [21].

## 2.6 The Kohn-Sham equations

The term  $\sum_{i<j}^N U(ri,rj)$  in equation 19 is what makes it hard to solve the Schrödinger equation, since many particles are involved in the interaction.

The Kohn-Sham (K-S) equation is the Schrödinger equation of non-interacting particles; that generates the same density as any given system of interacting particles. It is defined by a local effective fictitious external potential in which the non-interacting particles move, typically denoted as  $v_s(r)$  or  $v_{\text{eff}}(r)$ .

One can solve the so-called Kohn–Sham equations of this auxiliary non-interacting system,

$$\left[ -\frac{\hbar}{2m} \nabla^2 + \widehat{V}_s(r) \right] \phi_i(r) = \epsilon_i \phi_i(r) \quad (28)$$

where  $\epsilon_i$  is the orbital energy of the corresponding Kohn-Sham orbital (stata)  $\phi_i(r)$  and  $\widehat{V}_s(r)$  is an external effective potential in which the particles are moving.

Thus, the density for N-particle systems;

$$\rho(r) = \sum_{i=1}^N |\phi_i|^2 \quad (29)$$



The effective single- particle potential can be written in more details;

$$V_s(r) = V(r) + \int \left( \frac{e^2 n_s(r')}{|r-r'|} \right) d^3 r' + V_{xc}[n_s(r)] \quad (30)$$

Where:  $\int \left( \frac{e^2 n_s(r')}{|r-r'|} \right) d^3 r'$  is the so-called Hartree term describing the  $e - e$  coulomb repulsion.

$V_{xc}$  is called the exchange correlation potential.

The exchange interaction is a quantum mechanical effect between identical particles. It is due to the wave function of indistinguishable particles being subject to exchange symmetry that is either remaining unchanged (symmetric) or changing its sign (antisymmetric) when two particles are exchanged. Whereas the electronic correlation is the interaction between electrons in the electronic structure of a quantum system. The term  $V_{xc}$  is the summation of the exchange potential and the correlation potential [22].

## 2.7 The Exchange-Correlation Approximations

So far, we have seen the beautiful result of Kohn-Sham, which states that by finding a self-consistent solution to a set of single particle equations, will help us find the required ground state energy by minimizing the energy of an energy functional.

The main difficulty in solving the Kohn-Sham equation is with the exchange correlation (XC) term especially when dealing with an n body system, the problem becomes extremely complicated that needs super computers to be solved. Although HK theorems tells us that, there is an exchange correlation functional, it is still not known. For a good start, there is one system which is the uniform electron gas where the electron density is constant everywhere and the exchange correlation functional is

known. Using the uniform electron gas XC potential may not be of practical use since the electron density is the main feature that defines the chemical bonding. However, Kohn- Sham used the uniform electron gas XC potential locally which is called the local density approximation (LDA). The LDA allow us to completely define the Kohn-Sham equation but one should be careful since we are not solving the actual Schrödinger equation as a consequence of not using the correct XC functional.

LDA approximation is not the only used approximation. Scientists worked and are still working very hard to improve these approximated functional. For example, one of the best known functional uses the LDA approximation along with local gradient in the electron density which is known as the generalized gradient approximation (GGA), more detailed explanation will be given in chapter 3 about some functional that have been used within DFT which we will be using to carry out our study [23].

## **2.8 The Linearized Augmented Plane Wave Method**

The Linearized augmented plane wave (LAPW) method is one of the most accurate methods to solve the Kohn sham equation. It is used in most of the available computational software including the WIEN2K that we will be using in this work.

The LAPW method relies on dividing space into two regions as shown in (Figure 5). The first one is a non-overlapping atomic sphere and the other is the interstitial region around these spheres.

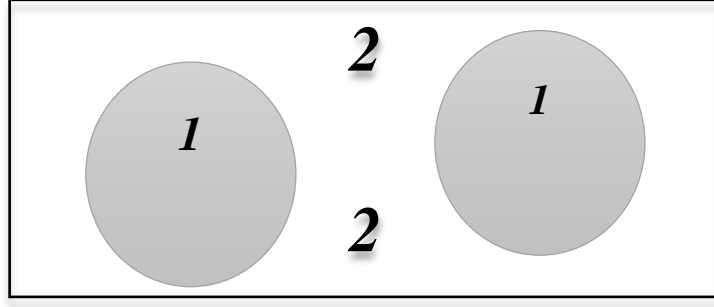


Figure 5: Division of the unit cell into two regions 1) the atomic spheres and 2) the interstitial region

Inside each atomic sphere of radius  $R$  the wave function  $\phi_{k_n}$  is a combination of radial functions times the spherical harmonics  $Y_{lm}(r)$ .

$$\phi_{k_n} = \sum_{lm} [A_{lm,k_n} u_l(r, E_l) + B_{lm,k_n} \dot{u}_l(r, E_l)] Y_{lm}(\hat{r}) \quad (31)$$

where  $u_l(r, E_l)$  is the regular solution of the radial Schrödinger equation (at the origin) for energy  $E_l$  taken at the center of bands with the corresponding  $l$ -like character.  $\dot{u}_l(r, E_l)$  is the energy derivative of  $u_l(r, E_l)$  taken at the same  $E_l$ .

Note that  $A_{lm,k_n}$  and  $B_{lm,k_n}$  are not variational constants, they are functions of  $k_n$  and are determined by requiring that the wave function is a continuous sphere's boundary.

In the interstitial region, the wave function takes a PW form:

$$\phi_{k_n} = \frac{1}{\sqrt{\omega}} e^{i\mathbf{k}_n \cdot \mathbf{r}}, \quad (32)$$

where  $\mathbf{k}_n = \mathbf{k} + \mathbf{K}_n$ .  $\mathbf{K}_n$  is the reciprocal lattice vector and  $\mathbf{k}$  is the wave vector inside the first Brillouin zone.

The solution of the Kohn Sham equation is taken to be the combination of the basis set of the LAPW according to the variational method.

$$\psi_{\mathbf{k}_n} = \sum_n c_n \phi_{\mathbf{k}_n} \quad (33)$$

where  $c_n$  are determined by the Rayleigh Ritz variational principle<sup>3</sup>.

To improve the wave function and to increase the flexibility of the basis the addition of one more ( $\mathbf{k}_n$  independent) term is necessary. This term is called the local orbital (LO) and it is used to ensure orthogonality. Local orbitals consist of two radial functions at two different energies that will make it possible to treat a semi core and valence states in one energy window consistently (for example 3s and 4s energies).

$$\phi_{lm}^{LO} = [A_{lm} u_l(r, E_{1,l}) + B_{lm} \dot{u}_l(r, E_{1,l}) + C_{lm} u_l(r, E_{2,l})] Y_{lm}(\hat{\mathbf{r}}), \quad (34)$$

The coefficients  $A_{lm}$ ,  $B_{lm}$  and  $C_{lm}$  by requiring that first:  $\phi_{lm}^{LO}$  should be normalized, second it should be zero at the boundaries of the sphere, third derivative should also be zero at the boundaries of the sphere [24]–[26].

## 2.9 Computation on Solids: Electronic Band Structure

The band structure is one of the most important concepts in solid-state physics; it shows the available energy ranges that the electron may have in a material and the forbidden energies, which the electrons cannot acquire. Each electronic level in the

---

<sup>3</sup> The Rayleigh Ritz variational principle deals with finding the Hamiltonian expectation value and try to minimize it. The Ritz theorem states that the expectation value of the Hamiltonian is stationary with respect to the neighbor space of its discrete eigenvalue.

band structure is characterized by the Bloch vector  $\mathbf{K}$  and the band index  $n$ . The Bloch vector is related to the reciprocal lattice and has the dimension of (1/ Length).

The band structure may give indications about the Fermi energy level, the band gap, type of the band gap – direct band gap or indirect band gap-, width of valence and conduction bands, etc.

This shows the need to be explicit about what is meant by the band structure, and to make it simple, let us assume a lattice in one dimension that may be generalized later into two and three dimensions easily. Imagine that we have  $N$  atoms resting at their lattice locations  $r_n = na$ , where  $a$  is the lattice constant and  $n = 1, 2, \dots, N$ . Assuming a periodic potential caused by the ions such that:

$$V_{tot}(x) = \sum_{n=1}^N V_a(x - na) \quad (35)$$

Where  $V_a(x)$  is the potential from an ion at the origin. Injecting this potential in Schrödinger's equation, we will get:

$$\left[ -\frac{\hbar^2}{2m} \frac{d^2}{dx^2} + V_{tot}(x) \right] \varphi(x) = E \varphi(x) \quad (36)$$

Using periodic boundary conditions  $\varphi(x + Na) = \varphi(x)$  such that the probability of being in any unit cell must be the same regardless of the unit cell and the wave function should vary inside the unit cell, we may guess that the wave function would take the following form:

$$\psi_k(x) = \frac{1}{\sqrt{N}} \sum_R e^{ikR} \varphi_k(x - R) \quad (37)$$

Where  $u_k(x)$  is periodic and  $k = \frac{2\pi}{Na}$

It is believed that this guess works perfectly and it is known as the Bloch wave functions, with the only distinct solutions come in the range of  $k \in [-\frac{\pi}{a}, \frac{\pi}{a}]$  which means in the first Brillouin zone.

The expectation value of the energy now reads;

$$E(\mathbf{K}) = \int \psi_k H \psi_k dx \quad (38)$$

Substituting equation 37 in equation 38 will give;

$$E(\mathbf{K}) = \frac{1}{N} \int \sum_R e^{-ikR} \varphi_k(x - R) H \sum_{R'} e^{ikR'} \varphi_k(x - R') dx \quad (39)$$

Taking  $x' = x - R$ , with the fact that our Hamiltonian is periodic (unchanged under translation  $H(x') = H(x)$ ) equation (36) becomes;

$$E(\mathbf{K}) = \frac{1}{N} \int \sum_R \varphi_k(x') H \sum_{R''} e^{ikR''} \varphi_k(x' - R'') dx' \quad (40)$$

Where  $R'' = R' - R$  is another translation vector. The summation over R will just give a factor of N and the final expression of the expectation value is now;

$$E(\mathbf{K}) = \sum_{R''} e^{ikR''} \int \varphi_k(x') H \varphi_k(x' - R'') dx' \quad (41)$$

Equation 8 is valid only for  $R''$  very small. Taking  $R'' = 0$ ;

$$E_{R''=0}(\mathbf{K}) = \int \varphi_k(x') H \varphi_k(x') dx' = \epsilon_s \quad (42)$$

The subscript s stands for the s orbital since we are interested in the ground state. Separating the  $R'' = 0$  term from equation 8, we will end up with an expectation value of two terms;

$$E(\mathbf{K}) = \epsilon_s + \sum_{\tau} e^{ik\tau} \gamma(|\tau|) \quad (43)$$

Where in second term we assumed the translation vector to be  $\tau = \pm a_o \hat{i}$  and  $\gamma(|\tau|) = \int \varphi_k(x') H \varphi_k(x' - \tau) dx$ .

$$E(\mathbf{K}) = \epsilon_s + \gamma(|\tau|) [e^{ika_o} + e^{-ika_o}]$$

$$E(\mathbf{K}) = \epsilon_s + 2 \gamma(|\tau|) \cos(ka_o) \quad (44)$$

Which shows that for an s orbital the energy varies with the k points as shown in (Figure 6) [27].

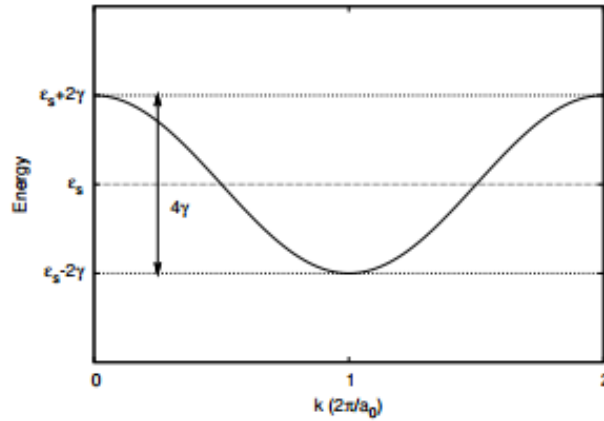


Figure 6: The  $E(\mathbf{K})$  relation for an S orbital,  $\mathbf{K}$  in the range  $[0, 2\pi a_o]$  with a band width of  $4\gamma$

Generalizing equation 44 to three dimension is now an easy task, it just requires a little algebra with  $\tau = \frac{a}{\sqrt{2}}$  the distance between two nearest neighbors in a face centered cube and  $k \rightarrow (k_x, k_y, k_z)$ . It will become:

$$E(\mathbf{K}) = \epsilon_s + 4 \gamma(|\tau|) \left( \cos\left(\frac{k_x a}{2}\right) \cos\left(\frac{k_y a}{2}\right) + \cos\left(\frac{k_y a}{2}\right) \cos\left(\frac{k_z a}{2}\right) + \cos\left(\frac{k_z a}{2}\right) \cos\left(\frac{k_x a}{2}\right) \right) \quad (45)$$

The bands of the different state orbitals of the electrons inside a crystal of an  $N$  atom will have  $N$  degenerate levels of each atomic state due to the interactions between the atoms and that is what creates the bands [28], [29].

## 2.10 Density of States

In solid state physics and condensed matter physics, the density of state of a system describes the number of states per interval of energy at each energy level that are available to be occupied by electrons. The task of calculating every possible carrier wave function as well as its corresponding energy is impractical. Fortunately, rather than solving the Schrödinger equation multiple times, we can instead find what is referred to as a density of states. This is when multiplied by an interval of energy, provides the total concentration of available states in that energy range. The Density of state is a very critical variable in the density functional theory.

Namely,

$$N(\text{interval}) = \rho(E)dE \quad (46)$$

where  $N$  is the total concentration of available states in the energy range  $dE$ , and  $\rho(E)$  is the desired density of state. We consider the case of a particle in a 3-D infinite potential box with  $V(x,y,z) = 0$  inside the box as shown in figure 7.

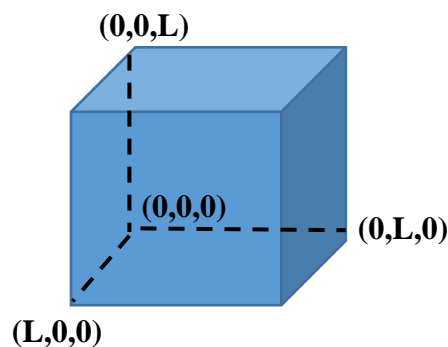


Figure 7: Electron in a box of length  $L$ . With  $V(x,y,z) = 0$  inside the box and  $\infty$  outside



The wave function and the energies obtained using Schrödinger equation is;

$$E(3D - box) = \frac{\hbar^2 K^2}{2m}, \quad (47)$$

where  $K^2 = \frac{n^2 \pi^2}{L^2}$  and  $n^2 = n_x^2 + n_y^2 + n_z^2$  are positive integers and  $L$  is the radius of the box.

Now, to find the density of state (DOS) we will work in the  $K$ -space where we will represent each quantum state as a dot as shown in figure 8.

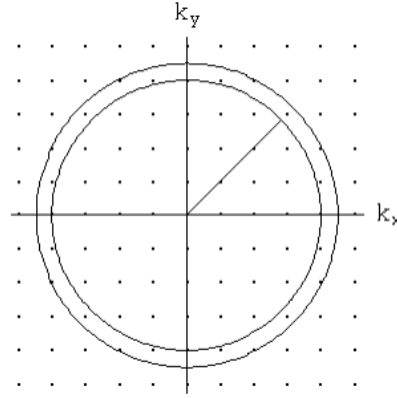


Figure 8: Two-dimensional array of allowed quantum states represented by the dots

To calculate the volume of one quantum state, one needs to find the spacing between two quantum states ( $K_{x+1}$  and  $K_x$ ) as shown in figure 7.

$$K_{x+1} - K_x = (n_x + 1) \left(\frac{\pi}{L}\right) - n_x \left(\frac{\pi}{L}\right) = \frac{\pi}{L} \quad (48)$$

Using equation (48) to find the volume of one quantum state leads to:

$$V_{QS} = \left(\frac{\pi}{L}\right)^3 \quad (49)$$

Dividing the volume of spherical shell of radius  $dK$  as shown in figure 8. by the volume of one quantum state will give the total number of available states;

$$N(\text{interval}) = 2 \frac{4\pi K^2 dK}{8 \left(\frac{\pi}{L}\right)^3} \quad (50)$$

where the factor 2 takes into account the two spin states allowed for each quantum state, the factor  $\frac{1}{8}$  deals with taking the octant of the sphere since we consider only positive values for  $K$ ,  $4\pi K^2 dK$  is the volume of the shell as shown in figure 9 and  $\left(\frac{\pi}{L}\right)^3$  is the volume of the quantum state.

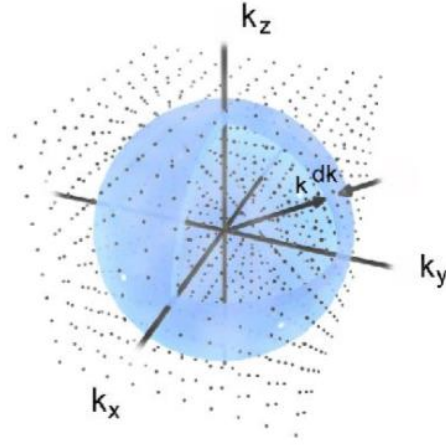


Figure 9: Positive octant part of the sphere for  $K_x, K_y, K_z > 0$

Comparing equation (50) to equation (46), we get.

$$\rho(K) dK = \frac{L^3 K^2 dK}{(\pi)^2} \quad (51)$$

$K$  and  $E$  are related; since we have

$$E(3D - box) = \frac{\hbar^2 K^2}{2m}$$

$$\frac{2mE}{\hbar^2} = K^2 \quad \text{and} \quad dk = \left(\frac{m}{\hbar\sqrt{2mE}}\right) dE \quad (52)$$

Equation (51) becomes:

$$\rho(E)dE = \frac{L^3}{(\pi)^2} \left(\frac{2mE}{\hbar^2}\right) \left(\frac{m}{\hbar\sqrt{2mE}}\right) dE \quad (53)$$

Arranging equation (53):

$$\rho(E)dE = \frac{4\pi L^3}{h^3} (2m)^{\frac{3}{2}} \sqrt{E} dE \quad (54)$$

where equation (54) gives the total number of quantum states in the region between  $E$  and  $dE$ . Dividing equation (54) by  $L^3$  we will get the density of quantum states per unit volume of the crystal as shown in equation (55).

$$g(E) = \frac{4\pi}{h^3} (2m)^{\frac{3}{2}} \sqrt{E} \quad (55)$$

The case of a particle in a 3-D infinite potential box is the simplest example that is used to explain the density of states. Different potential systems would have different density of states and this proportionality relation between  $g(E)$  and  $E$  would change as well [30], [31].

## Chapter 3: Exchange Correlation Potential

The difficulty in solving the Kohn Sham equation lies in the complication of defining the exchange-correlation potential. Density functional theory, in practical applications, is simple and accurate when compared to the experimental results. DFT approximations have shown excellent results in solving the Kohn sham equation. In this chapter, we will list some of these approximations.

### 3.1 The Generalized Gradient Approximation

#### 3.1.1 Introduction

So far, we referred to solving the Kohn Sham equation for N particles system by using the electron density as the main factor but can we do that in real systems. Using the density only was the approach used in local spin density approximation (LSD was the main approach to study the electronic structure for many years) which cannot be used in system of varying densities. John P. Perdew proposed a new approach in approximating the exchange-correlation potential by using the local density along with its gradient, so instead of using equation 56-a in the LSD approximation we can use equation 56-b:

$$E_{xc}^{LSD}[n_{\downarrow}, n_{\uparrow}] = \int d^3\mathbf{r} n(\mathbf{r}) \varepsilon_{xc}(n_{\downarrow}, n_{\uparrow}) \quad (56-a)$$

where  $n(\mathbf{r}) = n_{\downarrow} + n_{\uparrow}$  and  $\varepsilon_{xc}(n_{\downarrow}, n_{\uparrow})$  is the exchange correlation energy per particle.

$$E_{xc}^{GGA}[n_{\downarrow}, n_{\uparrow}] = \int d^3\mathbf{r} f(n_{\downarrow}, n_{\uparrow}, \nabla n_{\downarrow}, \nabla n_{\uparrow}) \quad (56-b)$$

From this point, researchers have been working to improve this approximation to be practical to solve a real N particles problem. The literature of density functional theory contains many approximations for the functional  $f(n_{\downarrow}, n_{\uparrow}, \nabla n_{\downarrow}, \nabla n_{\uparrow})$ , one of the most

important approximation is Perdew-Wang 1991(PW91)[32] which we will be using for calculating the potential via Vienna ab-initio simulation package, the other one is PBE that we will be using under GGA approximation within WIEN2k package.

### 3.1.2 Theory

The form that the exchange correlation energy per particle always starts from the uniform electron gas. The exchange correlation energy can be written in terms of the exchange correlation hole<sup>4</sup> as shown in equation 57.

$$E_{xc} = \int_0^\lambda d\lambda \int d^3r \int d^3r' \frac{n(\mathbf{r})n_{xc,\lambda}(\mathbf{r},\mathbf{r}')}{2|\mathbf{r}-\mathbf{r}'|} \quad (57)$$

where  $n_{xc,\lambda}(\mathbf{r},\mathbf{r}')$  is the exchange-correlation hole at coupling strength  $\lambda$ .

Using LSD, the exchange correlation hole is well approximated as using a uniform electron gas:

$$n_{xc,\lambda}(\mathbf{r},\mathbf{r}') \approx n_{xc}^{unif}[n_\downarrow, n_\uparrow; |\mathbf{r}-\mathbf{r}'|=0] \quad (58)$$

Since LSD works best locally, in the regions around the electrons vicinity [33]. The definition of the uniform electron gas density and exchange correlation energy are well established but researchers were interested to improve the notion of a gradient dependent functional  $f(n_\downarrow, n_\uparrow, \nabla n_\downarrow, \nabla n_\uparrow)$ .

One major approximation of the gradient dependent functional uses the second order density gradient expansion of the exchange correlation hole, which was used by Perdew-Wang 1991. This approximation has a problem since it describes systems of slowly varying density, it does not describe the uniform electron gas as satisfactory as

---

<sup>4</sup> Exchange-correlation hole is the region of space around an electron where the probability to find another electron approaches zero due to coulomb repulsion and Pauli Exclusion Principle.

the LSD does, and restrictions must be considered when dealing with semi local form of equation 56. PW91 has many other problems regarding the approximated  $f(n_{\downarrow}, n_{\uparrow}, \nabla n_{\downarrow}, \nabla n_{\uparrow})$ , the derivation of the functional is very tedious, complicated and over parameterized. In 1996, Perdew, Burke and Ernzerhof (PBE) developed new approach to find the exchange correlation energy. They started with GGA for correlation energy only:

$$E_C^{GGA}[n_{\downarrow}, n_{\uparrow}] = \int d^3r n [\epsilon_C^{unif}(r_s, \xi) + H(r_s, \xi, t)] \quad (59)$$

where  $r_s$  is the local Seitz radius<sup>5</sup> ( $r_s = \left(\frac{3}{4\pi n}\right)^{1/3}$ ),  $\xi = \frac{n_{\uparrow} - n_{\downarrow}}{n}$  is the relative spin polarization, and  $t = \frac{|\nabla n|}{2\phi k_s n}$  is a dimensionless density gradient. In the definition of the parameter  $t$ ,  $\phi(\xi) = \frac{[(1+\xi)^{2/3} + (1-\xi)^{2/3}]}{2}$  is a spin scaling factor,  $k_s = \sqrt{4k_F/\pi a_0}$  is the Thomas-Fermi screening wave number and  $a_0$  is Bohr radius.

The construction of the H contribution is done under several assumptions.

1. In the limit  $t \rightarrow 0$  (the slowly varying limit),  $H \rightarrow (e^2/a_0)\beta\phi^3 t^2$  where  $\beta = 0.066725$ . This assumption was studied by SHANG-KENG MA *et al.* by subtracting the Hartree-Fock energy from the exact energy [34].
2. In the limit  $t \rightarrow \infty$  (the rapidly varying limit),  $H \rightarrow -\epsilon_C^{unif}$  where the correlation term (equation 59) vanishes and the exchange density dominates.

These two assumptions (mainly) can be satisfied by the following ansatz:

---

<sup>5</sup> Local Seitz radius or Wigner- Seitz radius, the radius of the sphere with a volume equivalent to the mean volume per atom in the solid.

$$H = (e^2/a_o)\gamma\phi^3 \times \ln\left\{1 + \frac{\beta}{\gamma} t^2 \left[\frac{1+At^2}{1+At^2+A^2t^4}\right]\right\} \quad (60)$$

$$\text{where} = \frac{\beta}{\gamma} \left[ \exp\left\{-\frac{\epsilon_C^{unif}}{\gamma\phi^3 e^2/a_o}\right\} - 1 \right]^{-1}.$$

Under the uniform high density scaling ( $t \rightarrow 0$ )  $E_C^{GGA}[n_\downarrow, n_\uparrow]$  becomes:

$$E_C^{GGA} = -\frac{e^2}{a_o} \int d^3r n \gamma\phi^3 \times \ln\left[1 + \frac{1}{\chi s^2/\phi^2 + (\chi s^2/\phi^2)^2}\right] \quad (61)$$

where  $s = |\nabla n|/2k_F n$ . For  $s = 0$  we recover the uniform gas LSD and  $E_C^{GGA}$  reduces to  $-\infty$ .

On the other hand, the exchange energy is expressed as:

$$E_X^{GGA} = \int d^3r n \epsilon_x^{unif} F_X(s) \quad (62)$$

Such that we recover the uniform gas limit  $F_X(0) = 1$ . The exact exchange energy follows the spin scaling relationship:

$$E_X[n_\uparrow, n_\downarrow] = \frac{E_X[2n_\uparrow] + E_X[2n_\downarrow]}{2} \quad (63)$$

For a small density variation, the LSD does better job than the gradient approximation and to recover the LSD we must have for  $F_X(s) \rightarrow 1 + \mu s^2$  as  $s$  approaches zero and  $F_{XC}(r_s, \xi, s) \rightarrow F_X(r_s \rightarrow 0, \xi)$ .

PBE also discussed the importance of the Lieb-Osford bound:

$$E_X[n_\uparrow, n_\downarrow] \geq E_{XC}[n_\uparrow, n_\downarrow] \quad (64)$$

They assumed  $F_X(s) = 1 + \kappa - \frac{\kappa}{(1 + \frac{\mu s^2}{\kappa})}$  with  $\kappa=0.804$ . PBE approximation shows very

satisfying results compared to the PW91, as shown in table 1 they both give same

results however PBE is much easier to prove. PBE gives the researchers the chance of improving the GGA by adjusting the value of  $\kappa$ , which was done in 1998 by Zhang *et al* [35]. Where they used  $\kappa= 1.245$  and they compared their results with the original PBE as shown in (table 1) (revPBE represent Zhang *et al* work) and the adjustment showed better results.

Table 1: Atomization energy of some molecules in Kcal/mol ( 1eV = 23.06 Kcal/mol) using different approximations [35], [36]

Molecul	Molecular atomization energy (kcal/mol)			
	PW91	PBE	revPBE	Exact
<b>H<sub>2</sub></b>	105	104.5	105.3	109.2
<b>CH<sub>4</sub></b>	421	419.2	410.9	419.3
<b>NH<sub>3</sub></b>	303	301.0	293.4	297.4
<b>OH</b>	101	109.5	106.3	106.4
<b>H<sub>2</sub>O</b>	235	233.8	227.2	232.2
<b>HF</b>	143	141.7	137.8	140.8
<b>Li<sub>2</sub></b>	20	19.7	19	24.4
<b>N<sub>2</sub></b>	242	241	231.8	228.6
<b>O<sub>2</sub></b>	143	141.7	132.6	120.5
<b>Mean absolute error</b>	8	8.1	4.9	



Later from the same year Perdew, Burke and Ernzerhof replied to the adjustment done by Zhang *et al.* and they justified that the improvement of the parameter  $\kappa$  will improve the energy calculations only but no other factors such as the bond length (table 2). They suggested that users may employ LSD as a simple and of wide applicability density functional and at higher level use GGA (U =0.804) since their approximation is valid for both Quantum chemistry and condensed matter physics.

Table 2: Bond length in Bohr for some molecules using different approximations [37]

<b>Molecule</b>	<b>LSD</b>	<b>PBE</b>	<b>revPBE</b>	<b>Experimental</b>
<b>H<sub>2</sub></b>	1.447	1.418	1.413	1.401
<b>CH<sub>4</sub></b>	2.074	2.071	2.073	2.052
<b>N<sub>2</sub></b>	2.071	2.084	2.089	2.072
<b>NO</b>	2.169	2.189	2.196	2.175
<b>O<sub>2</sub></b>	2.279	2.306	2.313	2.281
<b>F<sub>2</sub></b>	2.618	2.672	2.685	2.678

## 3.2 Modified Becke-Johnson Scheme

### 3.2.1 Introduction

Despite the success of the local density approximation and the generalized gradient approximation discussed earlier, the problem with these two approximations is that they neglected the derivative discontinuity of the exchange correlation energy.

GGA set all the parameters other than those that appear in the LDA to be constant. Becke-Johnson potential is a semi-local method, which leads the KS states with results that are considered accurate compared to the experimental results.

The work done on this approximation started in 1983, A.D. Becke examined the short range variation of the Hartree Fock exchange density by performing taylor expansion[38]. In 1989, A.D.Becke and M.R.Roussel introduced a new exchange hole model (locally)  $v_{x,\sigma}^{BR}$ , where:

$$v_{x,\sigma}^{BR}(\mathbf{r}) = \frac{-(1-e^{-x}-\frac{1}{2}xe^{-x})}{b_{\sigma}(\mathbf{r})} \quad (65)$$

Where  $x = ab_{\sigma}$  for an arbitrary  $a$ ,  $b_{\sigma}(\mathbf{r}) = \left[ \frac{x_{\sigma}^3 e^{-x_{\sigma}}}{8\pi\rho_{\sigma}} \right]^{\frac{1}{3}}$ . Which was the starting point that the scientists tried to improve [39].

### 3.2.2 Theory

The Hartree Fock equation may be expressed as [40]:

$$-\frac{1}{2}\Delta\psi_{i\sigma} + [\mathbf{V}_{nuc} + \mathbf{V}_{el} + \mathbf{V}_{X\sigma}^{(i)}]\psi_{i\sigma} = \epsilon_{i\sigma}\psi_{i\sigma} \quad (66)$$

where  $\mathbf{V}_{nuc}$  is the nuclear attraction potential,  $\mathbf{V}_{el}(\mathbf{r}_1) = \sum_{\sigma} \int \frac{\rho_{\sigma}}{r_{12}} d^3\mathbf{r}_2$  is coulomb repulsion interaction and the exchange potential  $\mathbf{V}_{X\sigma}^{(i)}$  is written as;

$$\mathbf{V}_{X\sigma}^{(i)}(\mathbf{r}_1) = -\frac{1}{\psi_{i\sigma}^*(\mathbf{r}_1)\psi_{i\sigma}(\mathbf{r}_1)} \times \sum_j \frac{\int \psi_{i\sigma}^*(\mathbf{r}_1)\psi_{j\sigma}^*(\mathbf{r}_2)\psi_{j\sigma}(\mathbf{r}_1)\psi_{i\sigma}(\mathbf{r}_2)}{r_{12}} \quad (67)$$

The first attempt to simplify equation (67) was to replace the orbital  $\psi_{i\sigma(r_1)}$  dependent by the density  $\rho_{i\sigma} = |\psi_{i\sigma}|^2$  which was introduced by Slater [41].

Equation (67) may be written as:

$$\mathbf{V}_{X\sigma}^{(Slatter)}(\mathbf{r}_1) = -\frac{1}{\rho_{\sigma}(\mathbf{r}_1)} \times \sum_j \int \frac{\psi_{i\sigma}^*(\mathbf{r}_1)\psi_{j\sigma}^*(\mathbf{r}_2)\psi_{j\sigma}(\mathbf{r}_1)\psi_{i\sigma}(\mathbf{r}_2)}{r_{12}} \quad (68)$$

Another term can be defined now which is the exchange charge or the exchange hole:

$$\rho_{X\sigma}(\mathbf{r}_1, \mathbf{r}_2) = \frac{1}{\rho_{\sigma}(\mathbf{r}_1)} |\sum_i \psi_{i\sigma}^*(\mathbf{r}_1)\psi_{i\sigma}(\mathbf{r}_2)|^2 \quad (69)$$

Therefore,  $\mathbf{V}_{X\sigma}^{(Slatter)}$  can be:

$$\mathbf{V}_{X\sigma}^{(Slatter)}(\mathbf{r}_1) = -\int \frac{\rho_{X\sigma}(\mathbf{r}_1, \mathbf{r}_2)}{r_{12}} d^3\mathbf{r}_2 \quad (70)$$

The task now is to find a unique local potential that minimizes the total energy of the slater determinant proposed by Hartree Fock (this is known as the optimized effective potential). In 2006, A.D. Becke and E.R. Johnson found an approximation of the exchange potential that depends on the total density only. They found that the exchange potential is expressed as:

$$\mathbf{V}_X^{BJ}(\mathbf{r}) = \mathbf{V}_X^{BR}(\mathbf{r}) + \frac{1}{\pi} \sqrt{\frac{5}{6}} \sqrt{\frac{t_{\sigma}(\mathbf{r})}{\rho_{\sigma}(\mathbf{r})}} \quad (71)$$

where  $\mathbf{V}_X^{BR}(\mathbf{r})$  is the Becke- Roussel potential defined earlier,  $t_{\sigma}(\mathbf{r}) = \frac{1}{2} \sum_{i=1}^N \nabla \psi_{i,\sigma}^* \cdot \nabla \psi_{i,\sigma}$  and  $\rho_{\sigma}(\mathbf{r}) = \sum_{i=1}^N |\psi_{i,\sigma}|^2$  is the electron density [40].

In 2009, Tran and Blaha [42] proposed a modification on equation (71), as shown in equation (72). This was more accurate as shown in (table 3) when calculating the band gap of different solids.

$$V_{X\sigma}^{MBJ}(\mathbf{r}) = cV_{X\sigma}^{BR}(\mathbf{r}) + (3c - 2) \frac{1}{\pi} \sqrt{\frac{5}{12}} \sqrt{\frac{2t_{\sigma}(\mathbf{r})}{\rho_{\sigma}(\mathbf{r})}} \quad (72)$$

where:

$$c = \alpha + \beta \left( \frac{1}{V_{cell}} \int_{cell} \frac{|\nabla\rho(\mathbf{r}')|}{\rho(\mathbf{r}')} d^3\mathbf{r}' \right)^{\frac{1}{2}} \quad (73)$$

$V_{cell}$  is the unit cell volume.  $\alpha$  and  $\beta$  are two free parameters which were found according to experimental results, fitting to be -0.012 and 1.023 respectively while the band gap increases proportionally to the value of  $c$  [39].

Table 3: The value of the band gaps for several solids using different approximations along with the value of  $c$  calculated using equation (73)

<b>Solid</b>	<b>PBE</b>	<b>MBJ</b>	<b>Experiment</b>	<b>C</b>
<b>HfO<sub>2</sub></b>	4.09	5.83	5.7	1.44
<b>ZnS</b>	2.10	3.68	3.91	1.28
<b>ZnO</b>	0.82	2.71	3.44	1.42
<b>SiO<sub>2</sub></b>	6.01	8.89	10.30	1.47
<b>SrTiO<sub>3</sub></b>	1.88	2.7	3.25	1.41
<b>TiO<sub>2</sub></b>	1.89	2.57	3.3	1.44
<b>ZrO<sub>2</sub></b>	3.66	4.73	5.5	1.42
<b>Cu<sub>2</sub>O</b>	0.53	0.82	2.17	1.32

Table 3 shows that MBJ improves the calculated band gap except for Cu<sub>2</sub>O case where the band gap is underestimated. The value of  $c$  may affect the calculated band gap and it may be adjusted by hand to reach an optimized value that results a band gap that meets the experiment but that means equation (73) is not general enough,

though still the value obtained from equation (73) is not too far from the experimental values.

### 3.3 LDA+U

One major failure of the density functional theory and its exchange- correlation approximation is represented in the Mott insulators calculations. Other approximations were necessary to fit real problems of such materials.

In the Mott insulators systems, the repulsion force between the electrons is large enough to create a gap and change the conductivity features of the system as shown in figure 10. When the electron coulomb repulsion  $U$  is large enough (larger than the overlap  $W$ ), the electrons are forced to localize on atomic like orbitals (Mott localization).

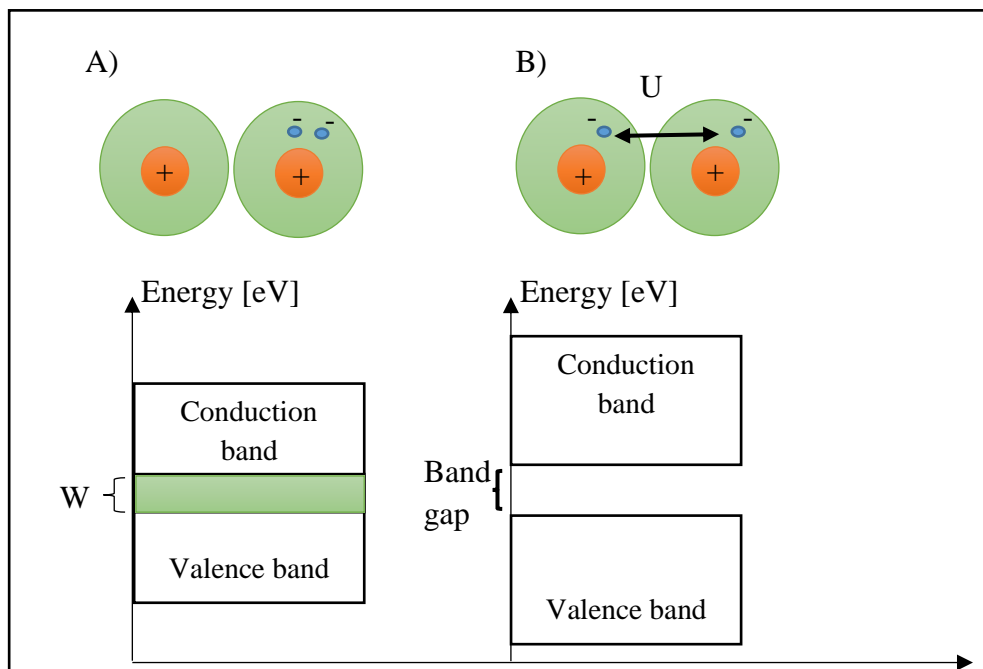


Figure 10: Schematic figure of the band gap a) The overlap between the valence and the conduction band with an overlap width  $W$  for metals. b) Shows the prevailing of the electrons coulomb repulsion on their Kinetic energy

This phenomenon requires a full knowledge of the multi determinant nature of the electron's wave function not the single determinant proposed by Hartree-Fock. Most of the known approximations (such as LDA and GGA) fail to represent the insulating nature of these systems. The main problem with analyzing these systems using the DFT approximation lies in the definition of the exchange – correlation potential, which aims to delocalize the electrons by the incomplete cancellation of the self- interaction between electrons in the coulomb integrals [43].

One way to solve the problem of a strongly correlated materials (such as the simple transition metal oxides) is by using the Hubbard model. This model strongly depends on the localized orbitals definition and determining the interaction parameters. The main assumption is that electrons of  $d$  and  $f$  orbitals, which are strongly correlated, are subject to a quasi-atomic interaction. Anisimov *et al.* defined the coulomb energy required to place two electrons on same site  $U$  and they corrected the known functional by adding a term which is called the Hubbard-like interaction  $E_{hub}$ :

$$E_{LDA+U}[n(\mathbf{r})] = E_{LDA}[n(\mathbf{r})] + E_{Hub}[\{n_m^{l\sigma}\}] - E_{DC}[\{n_m^{l\sigma}\}] \quad (74)$$

where  $n(\mathbf{r})$  is the electronic density,  $n_m^{l\sigma}$  are the atomic orbital occupations for the atom experiencing the Hubbard term and the last term is used to avoid double counting of the interaction in both  $E_{LDA}$  and  $E_{Hub}$ . On the other hand, they defined the Hubbard term with respect to the electron – electron repulsion potential as shown in equation (75):

$$\begin{aligned}
E_{Hub}[\{n_{mm'}^l\}] &= \frac{1}{2} \sum_{\{m\}, \sigma, l} \{ \langle m, m'' | \mathbf{V}_{ee} | m' m''' \rangle n_{mm'}^{l\sigma} n_{m''m'''}^{l-\sigma} \\
&+ (\langle m, m'' | \mathbf{V}_{ee} | m' m''' \rangle - \langle m, m'' | \mathbf{V}_{ee} | m''' m' \rangle) n_{mm'}^{l\sigma} n_{m''m'''}^{l\sigma} \} \quad (75)
\end{aligned}$$

With:

$$\langle m, m'' | \mathbf{V}_{ee} | m' m''' \rangle = \sum_{k=0}^{2l} \frac{4\pi}{2k+1} F^k \sum_{q=-k}^k \langle lm | Y_{kq} | lm' \rangle \langle lm'' | Y_{kq}^* | lm''' \rangle \quad (76)$$

where  $l$  is the angular momentum,  $F^k$  are the radial Slater integrals which are considered as the model parameters ( $k = 0, 1 \& 2$  corresponds to the  $d$  orbital, while  $k = 6$  is necessary when studying the  $f$  orbital). These parameters were redefined with respect to the Coulomb energy  $U$  and the exchange interaction  $J$  as follows:

$$U = \frac{1}{(2l+1)^2} \sum_{m, m'} \langle m, m' | \mathbf{V}_{ee} | m, m' \rangle = F^0 \quad (77)$$

$$J = \frac{1}{2l(2l+1)} \sum_{m \neq m', m'} \langle m, m' | \mathbf{V}_{ee} | m', m \rangle = \frac{F^2 + F^4}{14} \quad (78)$$

So that the double counting term will be expressed with respect to  $U$  and  $J$ :

$$E_{DC}[\{n_m^{l\sigma}\}] = \sum_l \frac{U}{2} n^l (n^l - 1) - \sum_l \frac{J}{2} [n^{l\uparrow} (n^{l\uparrow} - 1) + n^{l\downarrow} (n^{l\downarrow} - 1)] \quad (79)$$

Anisimov *et al.* proposed that the linearized muffin tin orbitals (LMTO's)<sup>6</sup> calculations can be performed on super-cells where the occupation of the localized

---

<sup>6</sup> LMTO's is an approximation used in LAPW where for LMTO's the potential has a spherical symmetric feature inside the muffin tin and constant in the interstitial region.

orbitals of one atom are restricted and limited as a start to run the calculations by dealing with atomic like problem [44].

In 1991, Anisimov *et al.* ran some calculations and compared the results of LSD with the results of LSD+U for the 3-d transition metal monoxides as shown in table 4 which shows clearly how the insulating feature using LSD+U.

Table 4: Band gap calculations for 3-d transition metal monoxides [14]

<b>Material</b>	<b>E<sub>LSD</sub></b>	<b>E<sub>LSD+U</sub></b>	<b>E<sub>exp</sub></b>
<b>CaCuO<sub>2</sub></b>	0	2.1	1.5
<b>CuO</b>	0	1.9	1.4
<b>NiO</b>	0.2	3.1	4.3
<b>CoO</b>	0	3.2	2.4
<b>FeO</b>	0	3.2	2.4
<b>MnO</b>	0.8	3.5	3.6

### 3.4 Hybrid Functional

The hybrid functional approach is a very successful in describing the molecular properties of large molecules and solids (especially metals). It depends on mixing part of the exact H-F exchange potential with the exchange- correlation potential from other sources (approximations). One approach was derived by Heyd and Scuseria in 2003, they developed a hybrid density functional based on a screened coulomb potential.



They split the coulomb operator into long range and short range (to avoid the divergence of the coulomb potential  $\frac{1}{r}|_{r=0}$ ) using the error function:

$$\frac{1}{r} = \frac{\text{erfc}(\omega r)}{r} + \frac{\text{erf}(\omega r)}{r} \quad (80)$$

where  $\frac{\text{erfc}(\omega r)}{r}$  indicates the short-range component and  $\frac{\text{erf}(\omega r)}{r}$  for the long-range component.  $\text{erfc}(\omega r) = 1 - \text{erf}(\omega r)$  and  $\omega$  is an adjustable parameter. For  $\omega = 0$  the long-range component vanishes and the short-range component is equivalent to  $\frac{1}{r}$  (the coulomb potential). Figure 11 [45] shows how this approximation (with  $\omega = 0$ ) let the exchange correlation energy decays exponentially with distance from the center of cell (just like the case for insulators where the exchange correlation potential decays exponentially as a function of the band gap [45])

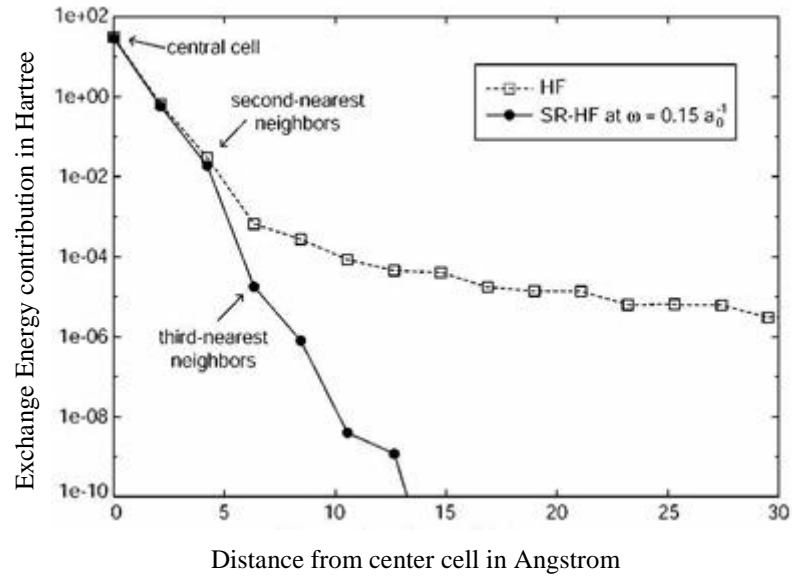


Figure 11: The decay properties of the screened coulomb potential (SR-HF) and the Hartree Fock potential. SR-HF decays exponentially with distance from center cell for carbon nanotube

They used the hybrid functional results obtained by Perdew, Ernzerhof and Burke who used their original GGA approximation PBE to determine a hybrid exchange-correlation energy  $E_{XC}^{PBE0}$  [46]:

$$E_{XC}^{PBE0} = aE_X^{HF} + (1 - a)E_X^{PBE} + E_C^{PBE} \quad (81)$$

Where  $a = \frac{1}{4}$  using perturbation theory.

Using the definition in equation (80) (splitting each term of the *exchange* potential in equation (81) to short range and long range) equation 81 becomes:

$$E_{XC}^{\omega PBEh} = aE_X^{HF,SR}(\omega) + (1 - a)E_X^{PBE,SR}(\omega) + E_X^{PBE,LR}(\omega) + E_C^{PBE} \quad (82)$$

Numerical calculations shows that the H-F and the PBE long range terms are very small for realistic values of  $\omega$ , so they cancelled [45].

In 2004, Heyd *et al.* assessed the Heyd-Scuseria-Ernzerhof (HSE) screened coulomb hybrid functional and calculated the band gap for several semiconductors and compared it with other approximations as shown in table [47].

Table 5: Band gaps in [eV] for four semiconductors with three different numerical approximations and experimental results

<b>Material</b>	<b>LDA</b>	<b>PBE</b>	<b>HSE</b>	<b>Experiment</b>
<b>C</b>	4.13	4.1	4.16	5.48
<b>Si</b>	0.52	0.71	0.78	1.17
<b>BN</b>	4.38	4.45	4.47	6.4
<b>BP</b>	1.23	1.35	1.41	2.4
<b>MAE<sup>a</sup></b>	1.3	1.32	1.27	

a: means absolute error

## Chapter 4: Methodology

During the past, decades computer simulations based on density functional theory and other quantum mechanical theories improved the material study field. The development of such packages that manage to solve the Kohn Sham equation with high efficiency and accuracy is not an easy task. In 1998, Walter Kohn shared the Nobel Prize for chemistry, in recognition of his work in developing DFT, with John Pople for developing the GAUSSIAN program package. The GAUSSIAN package is very important to perform accurate DFT calculations for complex molecular systems until today and the work on developing an equivalent package for solid state and material science is an active field.

In this work, we have used the density functional theory implemented in WIEN2k package (Version 14.2) and the Vienna ab-initio simulation package VASP (Version 5.3).

### 4.1 WIEN2k Package

WIEN2k is a Fortran program that uses the full potential linearized augmented plane wave to solve the Kohn-Sham equation and allows you to study various properties of the material under study such as density of state, electron density, band structure, optical properties, etc. Calculations with WIEN2k takes several steps starting with building your structure, then initializing the calculations to guess an initial density of electrons using a specific exchange correlation approximation, after that we run the self-consistent cycle until we reach convergence so that at the end we may run the desired study.

In this work, we have used the parameters in table 6 to build our structure as shown in figure 9. The geometric optimization was performed with the generalized gradient approximation (PBEsol-GGA) developed by Perdew, Burke and Ernzerhof in 1998 [35], [36].

Using equation (83) for the volume of the unit cell, the optimized lattice constants were found.

$$V = a^2 c \sin 60$$

$$V = ar \sin 60 \quad (83)$$

where  $r = \frac{c}{a}$ .

Table 6: The parameters used to build the molybdenum disulfide structure

Parameter	Value
<b>Title</b>	MoS <sub>2</sub>
<b>Space group</b>	P63/mmc, No 194 (2H)
<b>Lattice constants</b>	a=b=3.16 Å , c=12.29Å
<b>Angles</b>	A=β=90°      γ = 120°
<b>Position of atoms</b>	Mo: x= 2/3   y= 1/3   z= 1/4  S: x= 1/3   y= 2/3  z=0.1215

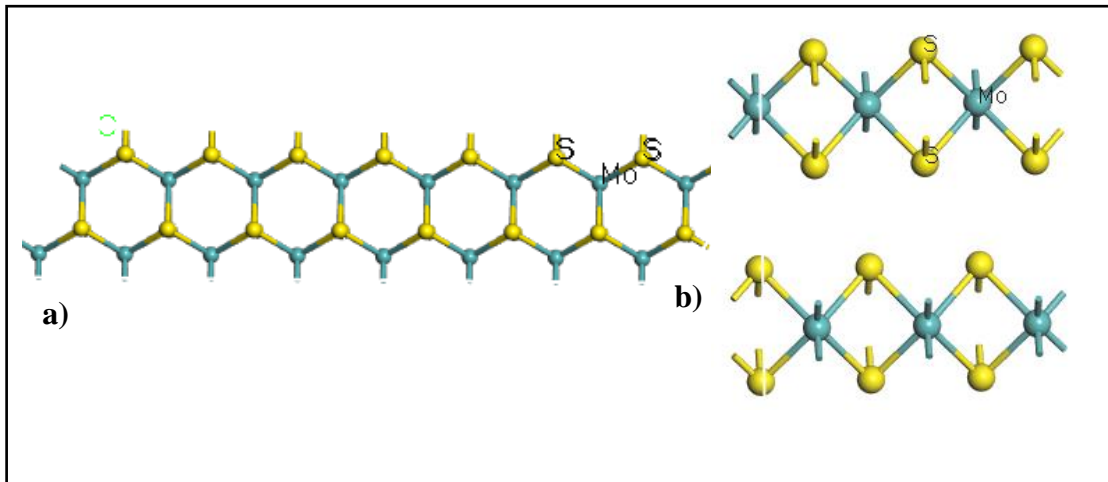


Figure 12: The crystal structure of a) Monolayer MoS<sub>2</sub> b) Bulk MoS<sub>2</sub>, the hexagonal lattice is clear

After rebuilding the structure with the optimized lattice constants, the exchange correlation function we calculated using different approximations including the generalized gradient approximation (PBEsol-GGA, Perdew08), The modified Becke-Johnson, GGA+U and the onsite Hybrid functional to test their performance. After running the self-consistent cycle for each approximation, the density of state and the band structure were plotted and calculated for the following structures:

1. Bulk Molybdenum disulfide [MoS<sub>2</sub>] (Figure 12.b).
2. Monolayer Molybdenum disulfide [ ML\_MoS<sub>2</sub>] (Figure 12.a).
3. MoS<sub>2</sub> with certain impurities including H, N and B (Figure13.a.b.c respectively).
4. Study the effect of pressure on the band gap.

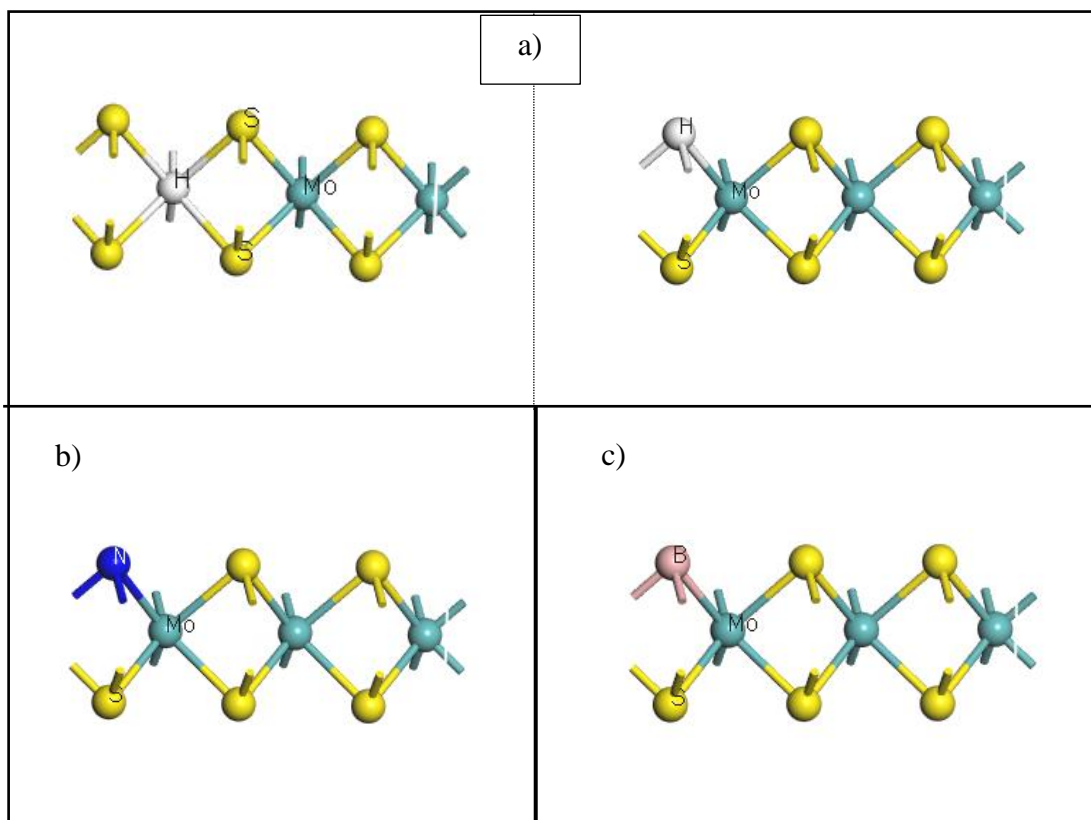


Figure 13 Interstitial substitution crystallography a) Hydrogen atom substitution in Sulfur vacancy b) Nitrogen substitution in Sulfur vacancy c) Boron substitution in Sulfur vacancy

## 4.2 VASP

VASP is a computer simulation for electronic structure calculation in the atomic scale based on LAPW and pseudo potentials (projector augmented wave method PAW)<sup>7</sup>. It approximates the solution of the Schrödinger equation within DFT by iterative matrix diagonalization technique. VASP is a very efficient software package for materials simulations, it was used to treat a system of 2744

<sup>7</sup> PAW is a technique used in ab initio electronic structure to generalize LAPW and the pseudopotential (effective potential).

(which is an extremely large supercell) atoms for simulating C defect in group 3 nitrides [48].

The most useful feature of this package is that it allows answering questions that are not applicable using the laboratory experiments. One major example is the study of the magnetic ordering in a nanostructured material (Nano-structured material has different magnetic properties than their bulk) since the information on the local magnetic moment cannot be achieved experimentally [49].

There are many exchange-correlations functional that are implemented in VASP such as GGA, LDA+U, HF, meta-GGAs, etc. In this thesis, we will be using the first three approximations to perform our calculations. It requires four input files to start the calculations, which are:

- 1) INCAR, it is the most important file during the calculations and it contains many parameters that are adjusted to meet the study objectives either for calculating the band structure, DOS or other features (usually kept as default for the complexity of this file).
- 2) POTCAR, this file contains the pseudo potential of each atom in the structure. In this study, pseudo potential is calculated using potPAW\_PW91).
- 3) KPOINT, it contains the K points coordination and the mesh size (Monkhorst-Pack MP). I used 5x5x1 and 10x10x2 for geometry optimization and DOS calculations respectively.
- 4) POSCAR, this file contains the geometry and the atomic positions; I used Materials studio program to create the POSCAR files for my structure shown in figures 12 and 14.

Before running any calculations, We calculated the equilibrium (optimized) lattice constants just like I did using WIEN2k, the optimized K points (mesh size) and we used the default cutoff energy of 400 [50].

We used VASP to study the electronic properties of Bulk  $\text{MoS}_2$ , Mololayer  $\text{MoS}_2$  and  $\text{MoS}_2$ - $\text{WSe}_2$  heterostructure figure 14.

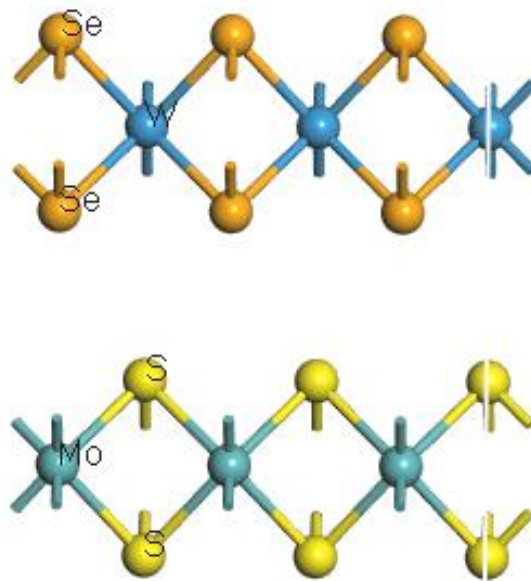


Figure 14:  $\text{MoS}_2$  -  $\text{WSe}_2$  Heterostructure



## Chapter 5: Results and Discussion

### 5.1 Optimization

The first step of this study is to find the equilibrium optimized lattice constants of our structure to build our cells (in both Wien2k and VASP). Using the experimental values of the lattice constants ( $a$  and  $c$ ) [51], energy versus  $c/a$  was plotted to find the optimum value that corresponds to the minimum energy for WIEN2k calculations and energy versus volume was plotted to find the optimized volume for the VASP calculations (Figure 15). The constants were calculated using equation 83 as shown in table 6.

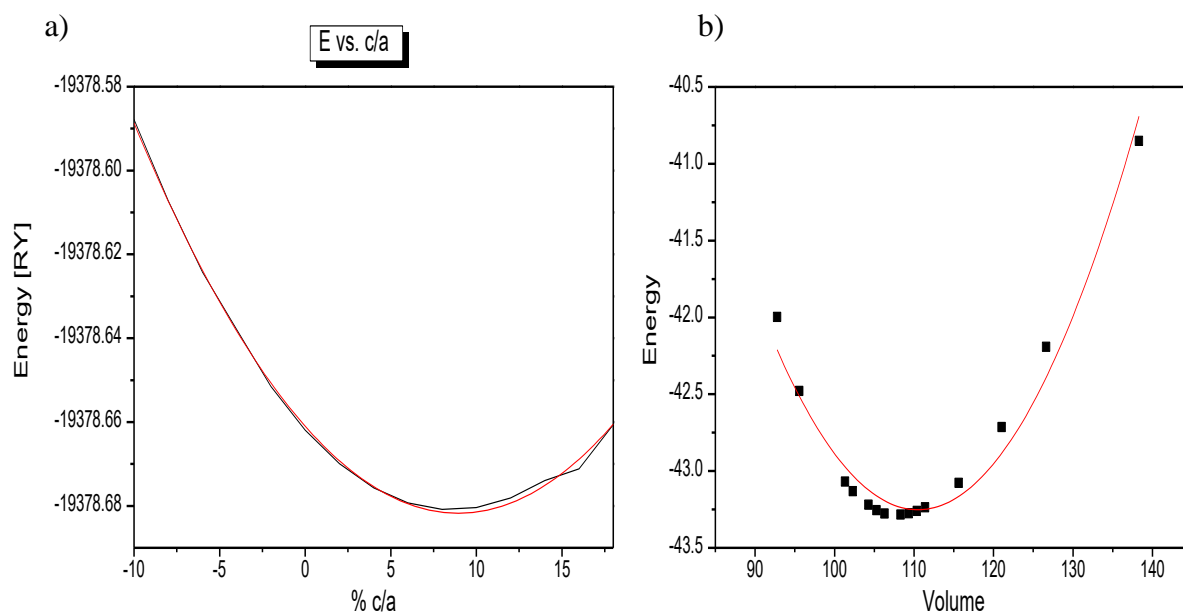


Figure 15: Optimization a) Energy in Rydberg [Ry] versus  $c/a$  % using WIEN2k to find the optimized lattice constants b) Energy versus volume using VASP to find the optimized volume and lattice constants

Table 7: The lattice parameters (a,b and c) using WIEN2k and VASP with the mean absolute error

Parameter	WIEN2k	VASP	Experiment [52].
<b>a=b</b>	3.07 (Å)	3.178(Å)	3.16(Å)
<b>C</b>	13.317(Å)	12.62(Å)	12.294(Å)
<b>c/a</b>	4.338	3.971	3.890
<b>V<sub>o</sub></b>	108.696 (Å <sup>3</sup> )	110.381(Å <sup>3</sup> )	106.316(Å <sup>3</sup> )
<b>MAE</b>	0.985	1.1225	-

An extra optimization using VASP have been used to find the optimum mesh size as shown in figure 16. The saturated mesh size to be 5×5×1.

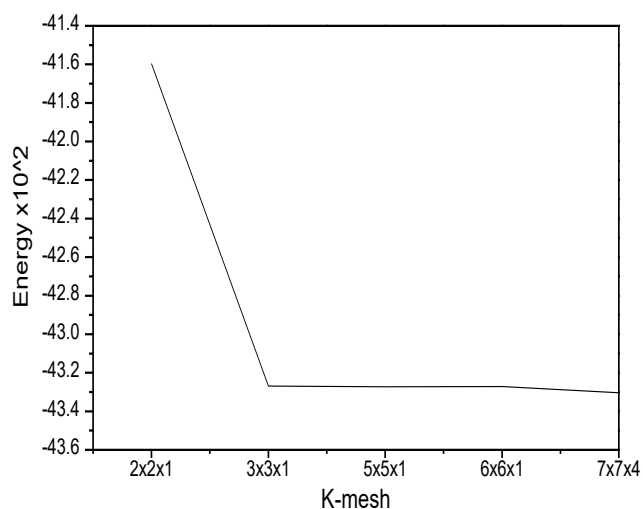


Figure 16: Energy versus K-mesh points to find the optimized k-mesh. K mesh saturates at 3×3×1

We used the default cut off energy, which was 400 eV. Using these optimized parameters, we rebuilt our structures and used the new files to run our calculations in sections 5.2 – 5.4.

## 5.2 Electronic Structure Calculations

Electronic structure calculations were performed by the two simulations (WIEN2k and VASP) using different approximations (GGA, MBJ, LDA +U and On-site Hybrid functional).

### 5.2.1 Bulk MoS<sub>2</sub> Calculations

The electron density along the plane (110) is displayed in Figure 17, which shows that the electrons are more concentrated along the molybdenum atom than the Sulfur atom.

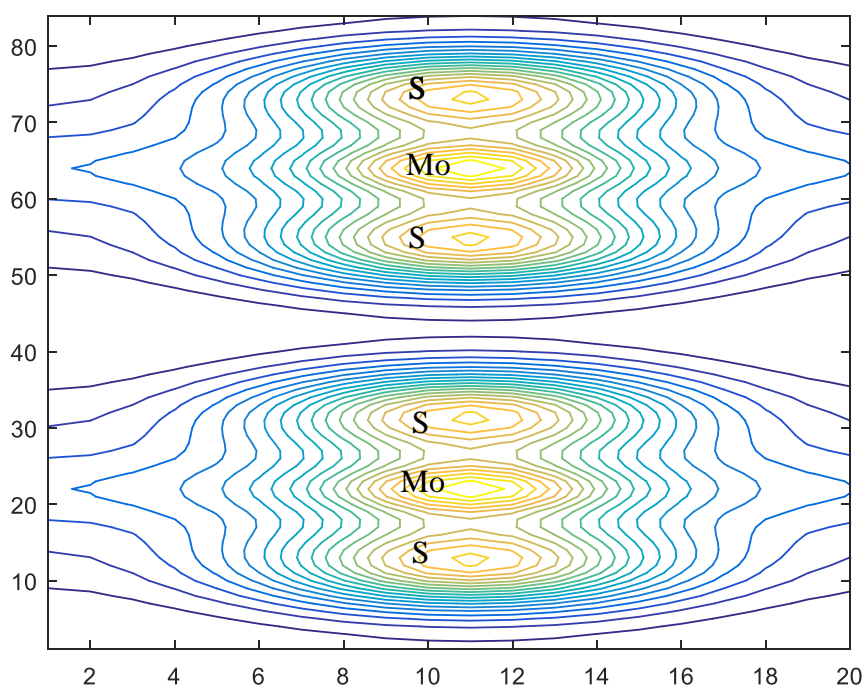


Figure 17: Electron Density around MoS<sub>2</sub> along the plane (110). The density of the lines indicates the electrons density

Four approximations were used to find the band gap of the bulk MoS<sub>2</sub> which are GGA, LDA+U, on-site hybrid functional and MBJ implemented in the WIEN2k package as shown in Figure 18 and 19. However, only three approximations were used (GGA, LDA+U and onsite hybrid functional) implemented in VASP as shown in figure 20.

The band gap of the bulk MoS<sub>2</sub> shows a clear indirect band gap semiconductor ( $\Gamma \rightarrow K$ ). The results are close to the experimental values obtained by Mak.K.F *et al* [53] where they found that the bulk MoS<sub>2</sub> has an indirect band gap of 1.23 eV. While MBJ approximation shows the most accurate results in WIEN2k package, the on-site hybrid functional shows the most accurate result in VASP package as shown in table 8. The failure of GGA to produce an accurate result was predicted because, as we mentioned earlier, GGA fails with TMID's due to Mott localization and it underestimates the band gap.

VASP produces more accurate results than the WIEN2k package does comparing the percentage differences with respect to the experimental value with 12.03 % more accuracy in the GGA approximation.

Table 8: The band gap of the bulk MoS<sub>2</sub> using different approximations implemented in both VASP and WIEN2k package

<b>Approximation</b>	<b>WIEN2K</b>	<b>VASP</b>	<b>% difference (WIEN2K)</b>	<b>% difference (VASP)</b>
<b>GGA</b>	0.898	1.015	31.99	19.96
<b>LDA+U</b>	0.999	1.024	21.52	19.1
<b>On-site Hybrid functional</b>	0.986	1.501	22.8	18.98
<b>MBJ</b>	1.176	-	5.29	-

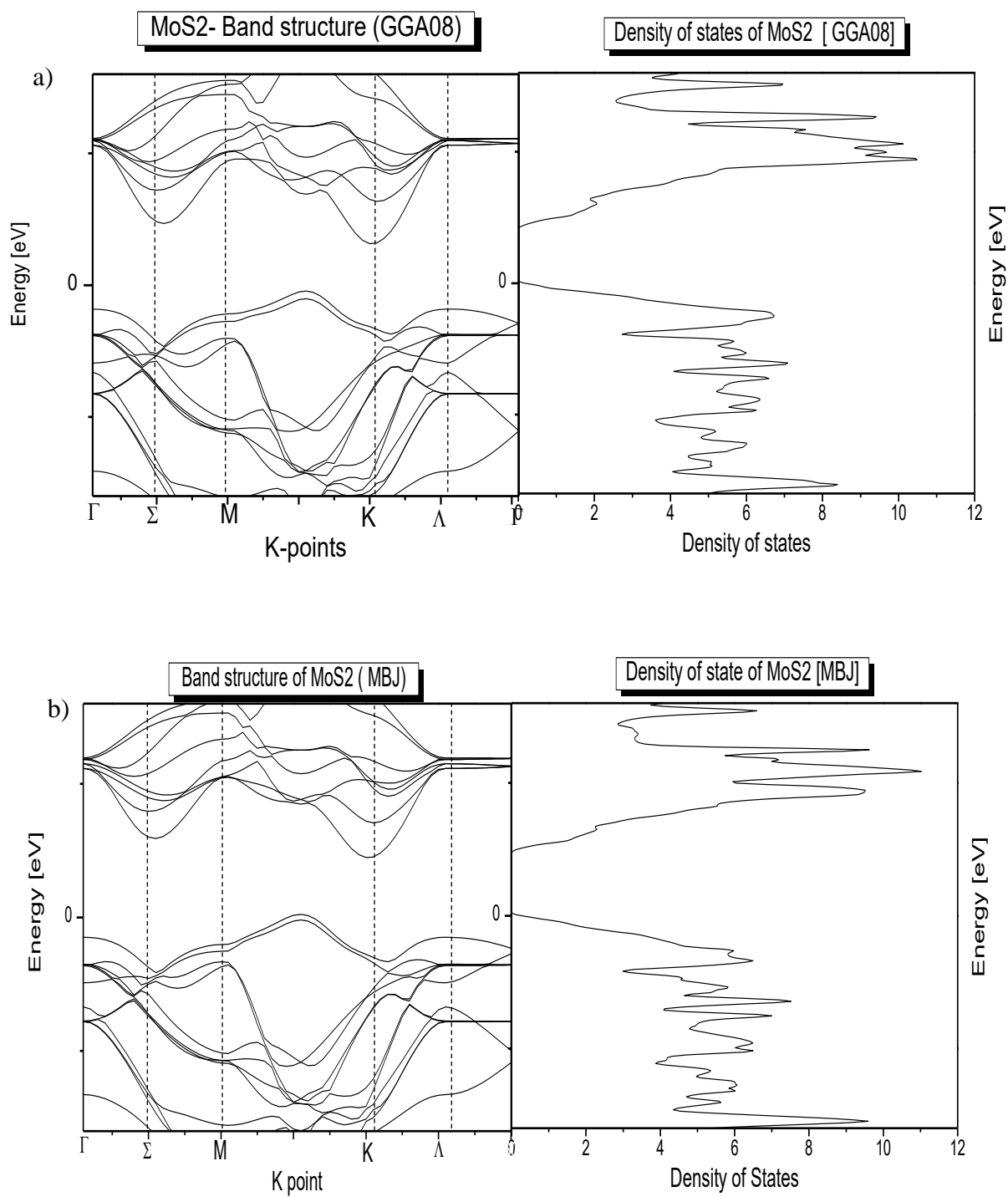


Figure 18: The band structure (left) and DOS (right) of bulk MoS<sub>2</sub> using a) GGA  
b) MBJ

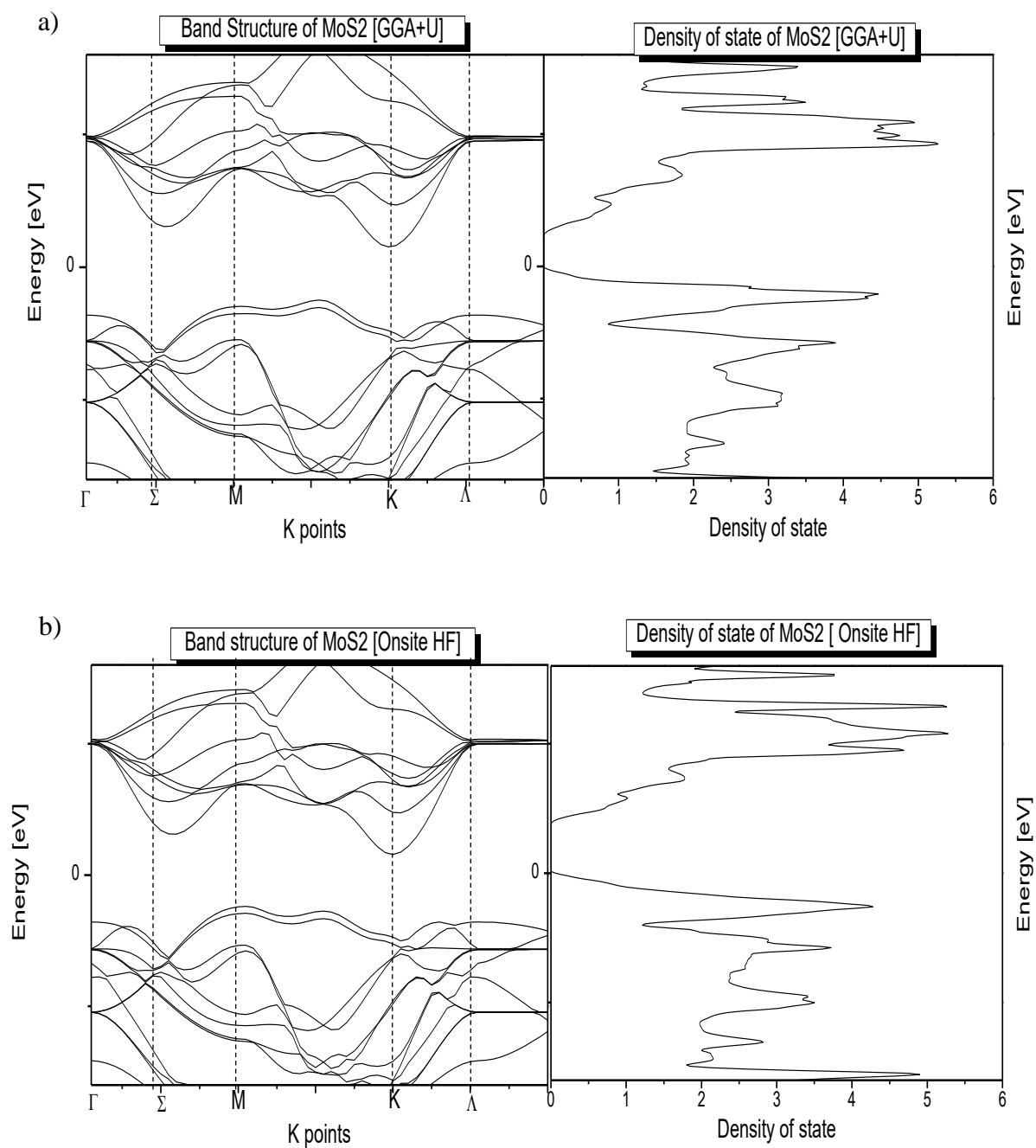


Figure 19: The band structure (left) and DOS (right) of bulk MoS<sub>2</sub> using a) LDA+U b) On Site Hybrid functional

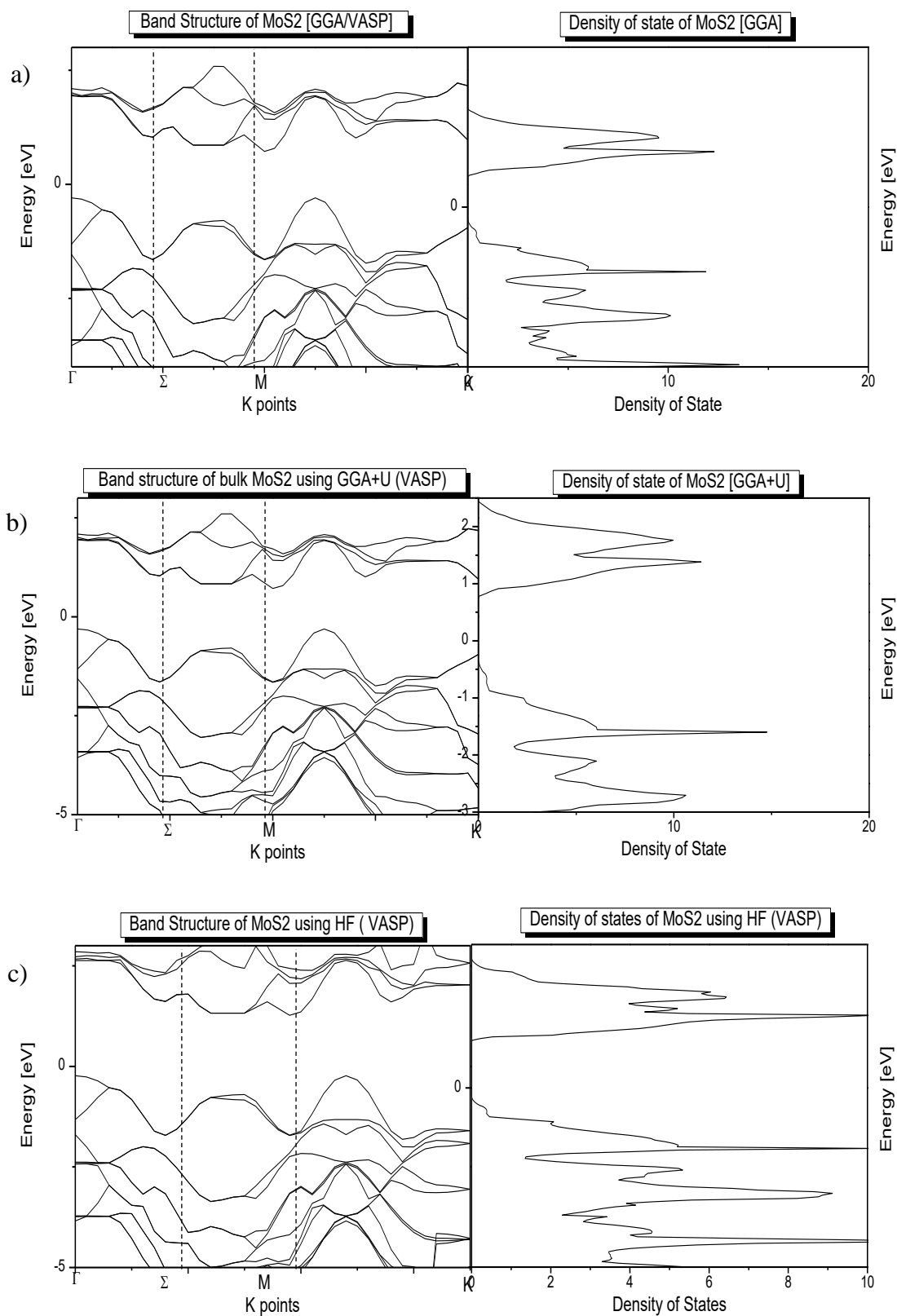


Figure 20: The band structure (left) and DOS (right) of bulk MoS<sub>2</sub> using a) GGA b) LDA+U c) on-site hybrid functional implemented in VASP which shows an indirect band gap



### 5.2.2 Monolayer MoS<sub>2</sub> Calculations

We used monolayer MoS<sub>2</sub> super-cell of size 2×2×1 to run my calculations with lateral size of 6.14×6.14 and 6.36×6.36 for WIEN2k and VASP respectively (4 Mo atoms and 8 S atoms). I found that the band gap changes from an indirect band gap (the case of the bulk) to a direct band gap and it widens. Figure 21 shows the band structure obtained by WIEN2K using different approximations while figure 22 shows the VASP results. VASP shows less percentage difference compared to the WIEN2k results where the difference was approximately 5% using the VASP simulation with respect to the experimental value of 1.8 eV[53].

Fermi level was also calculated using VASP simulation. Comparing Fermi levels of the monolayer MoS<sub>2</sub> with the bulk, a major reduction in the highest occupied state occurs (from 6.19 to 1.709 eV using GGA) [54].

Table 9: Band gap and fermi energy level for monolayer MoS<sub>2</sub> using different approximations

<b>Approximation</b>	<b>WIEN2k</b>	<b>VASP</b>	<b>% difference (WIEN2k)</b>	<b>% difference (VASP)</b>
<b>GGA</b>	1.325	1.7096	30.4%	5.19%
<b>LDA+U</b>	1.2903	1.711	33%	5.07%
<b>On-site hybrid functional.</b>	1.31	-	31.51%	-

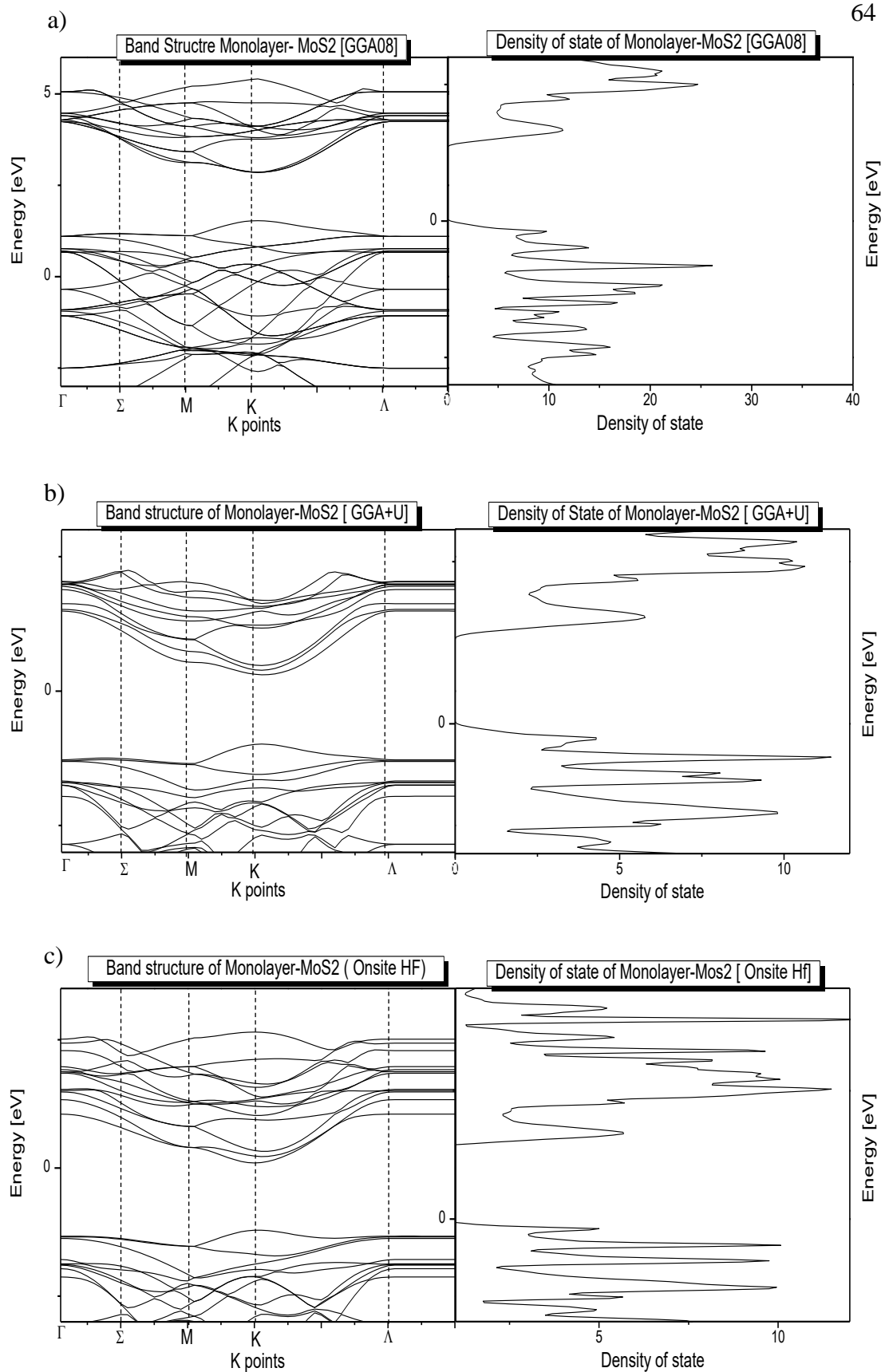


Figure 21: The band structure (left) and DOS (right) of monolayer MoS<sub>2</sub> using a) GGA b) LDA+U c) onsite Hybrid functional implemented in WIEN2k, which shows a direct band gap

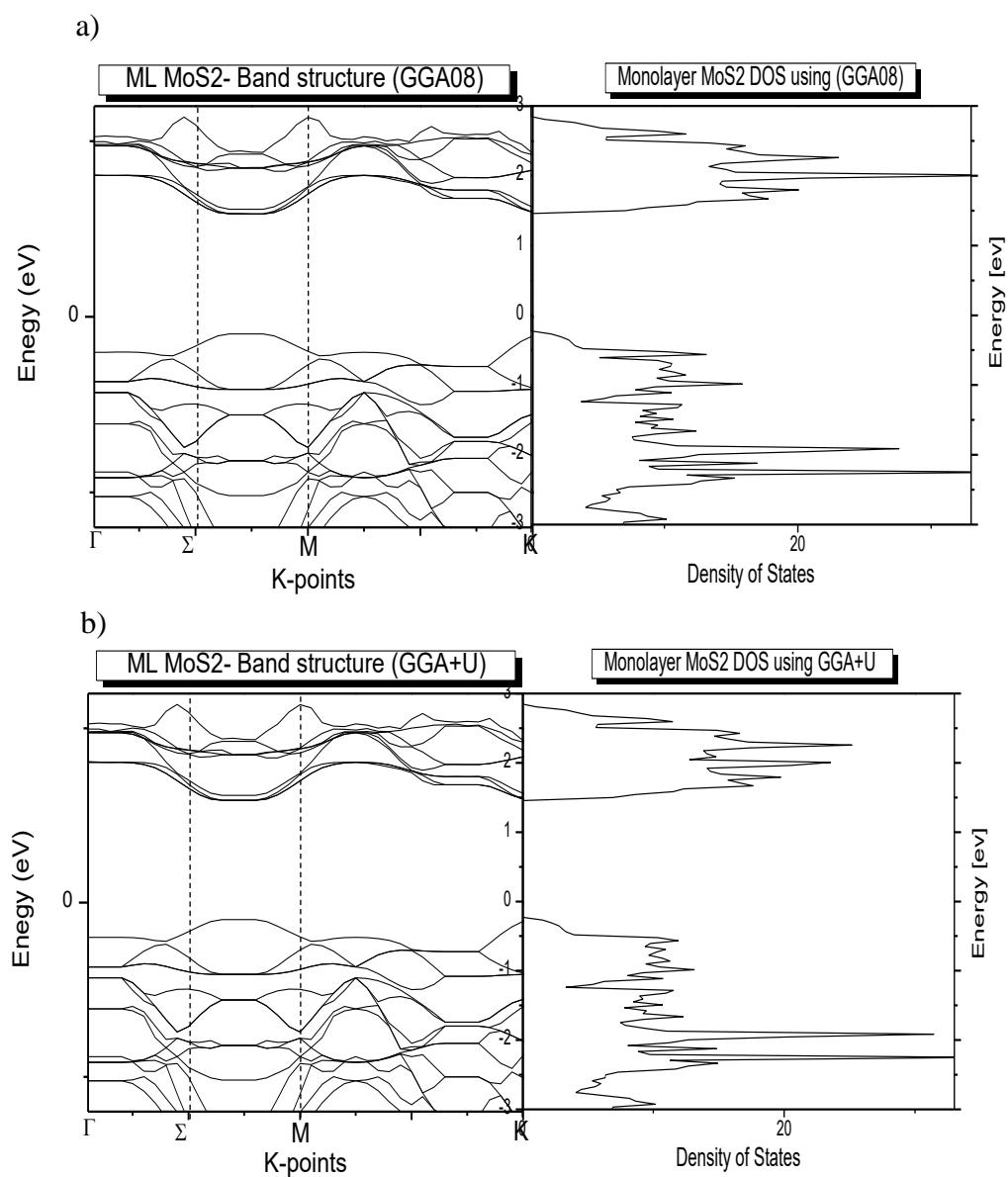


Figure 22: The band structure (left) and DOS (right) of monolayer MoS2 using a) GGA b) LDA+U implemented in VASP, which shows a direct band gap

### 5.2.3 Partial Density of States

Plotting the partial density of states for the valence orbitals of the molybdenum and the sulfur atoms (Figure 23) shows the contribution of each orbital in the density of states. Equations 84 and 85 shows the orbitals of the valence band for the atoms. As predicted, the  $d$  orbital has the most contribution in the density of states and the  $s$  orbital is barely showing. Comparing the different approximations there is a band missing in the GGA+U approximation (beyond 5 [eV]) and is showing clearly in the other approximations which may be due to the localization and the repulsion from coulomb interaction ( $U$ ) of the LDA+U approximation.

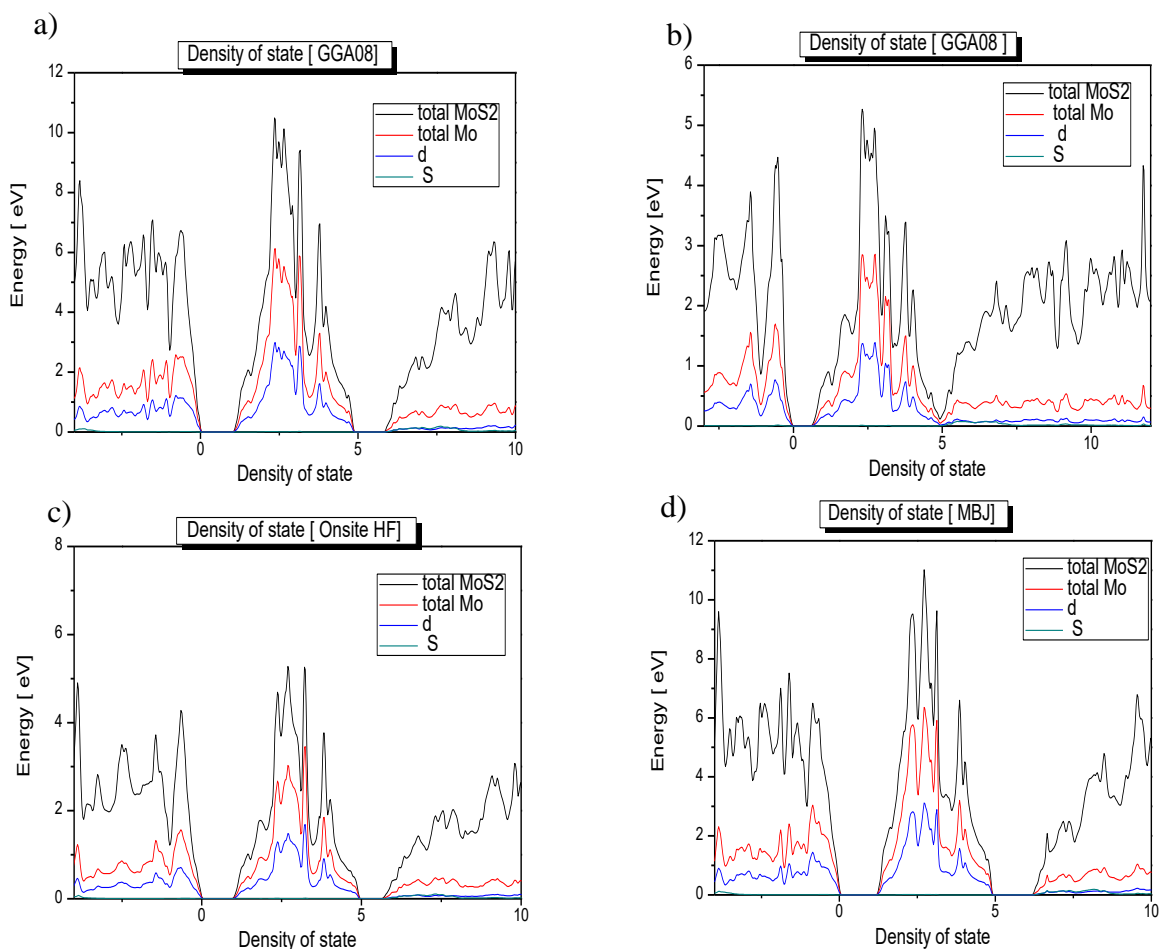


Figure 23: Partial density of states for the molybdenum atom and its  $s$  and  $d$  orbitals using a) GGA08 b) GGA+U c) onsite hybrid functional d) MBJ

The partial density of states for the sulfur atom are shown in figure 24. The contribution of the sulfur atom is less than the contribution of the molybdenum atom but the same feature appears in the GGA+U with the missing band beyond 5 eV. For the sulfur atom, the p orbital contributes more than the s orbital. For both atoms, GGA and MBJ shows more states than does the other two approximations and it may be due to the delocalization of inherent these approximations.

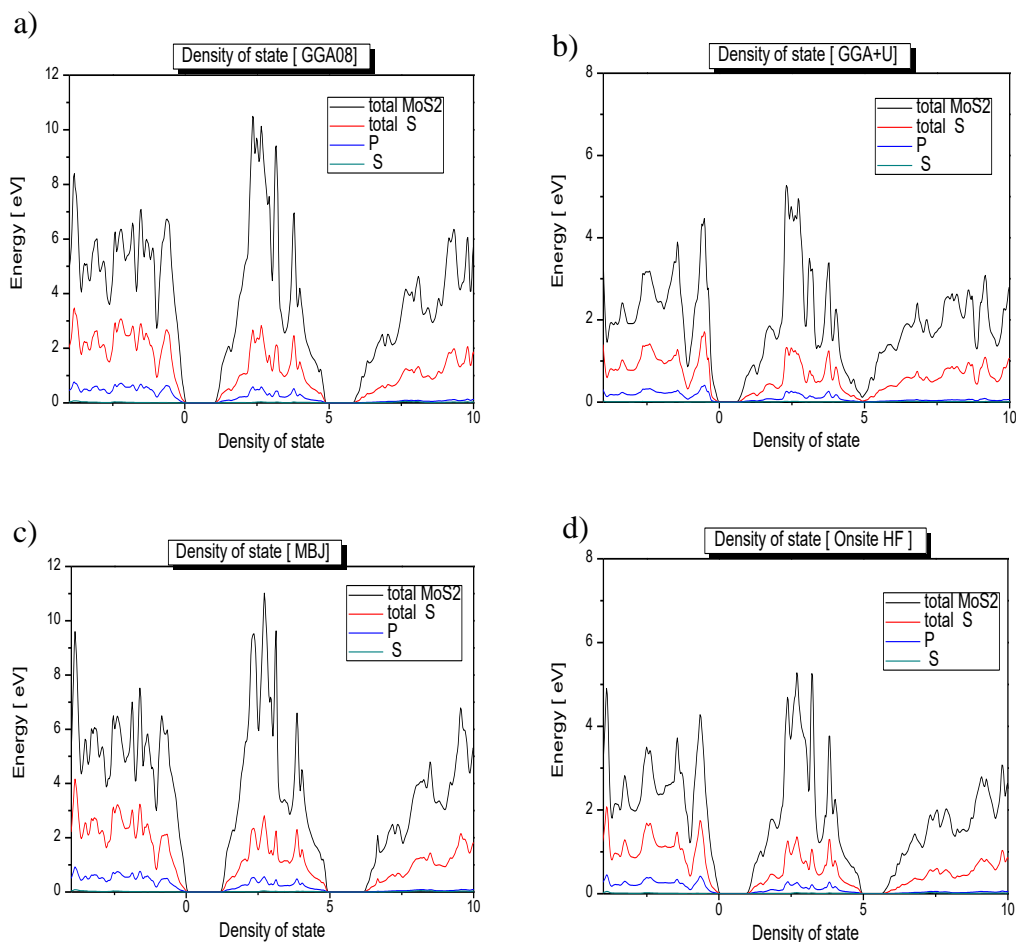
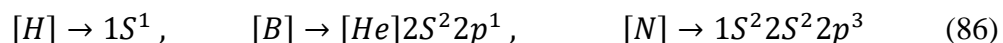


Figure 24: Partial density of states for the Sulfur atom and its s and p orbitals using a) GGA08 b) GGA+U c) onsite hybrid functional d) MBJ

### 5.3 Effect of Interstitial Substitution and Heterostructure on the Electronic Properties

Previous studies have shown that adsorption of non-metal (insulators and semiconductors) material on a small system (dimensionally small such as the 2D MoS<sub>2</sub>) will induce a magnetic moment. In 2010, He and his coworkers calculated the magnetic moment for several non-metal atoms adsorbed monolayer MoS<sub>2</sub>. They found that the magnetic moment of H-, B-, N- adsorbed Monolayer MoS<sub>2</sub> are 1.0, 1.0, 1.0 per 4x4 super cell respectively. In this study, I will investigate the effect of these dopants on the band gap of Monolayer MoS<sub>2</sub> will be investigated. The electronic configuration of the Hydrogen, Boron and Nitrogen are shown in equation (86).



As shown in figures 25, 26 and 27, the substitution of boron in sulfur vacancy (done initially using no spin polarization within GGA), The bands retain their band gap but other bands were created inside the gap itself which is consistent with the previous results of Yue. *et al.* and He. *et al.*[50], [55]. The substitution of boron caused a transition to the metallic phase, as Yue proposed, this may give a chance for spin separations or filtering, so a second calculation was done taking the spin polarization into account and performing the LDA+U approximation for the exchange - correlation potential. The results show that for the up spin channel a direct band gap is detected just like Yue's results but with an extra band which is due to the Hubbard potential and the repulsion coulomb interaction that is absent in GGA used by Yue. However, the down spin channel shows bands in the middle of the gap shifting the semiconductor behavior to a metallic behavior.

The Nitrogen substitution in a Sulfur vacancy shows a clear direct band gap just like the pure monolayer MoS<sub>2</sub> with a reduction in the band to reach 1.3 eV. While the Hydrogen atom was substituted in S vacancy and its band structure shows a metallic behavior just like the Boron substitution, so a spin polarized calculations using LDA+U was performed. The up-spin channel shows a direct band gap of 0.71 eV which is less than half the monolayer band gap with a valance band maximum of -0.68566 [eV] and a conduction band minimum of 0.028 [eV]. The down spin channel showed a similar direct semiconductor behavior with a band gap equals 0.709 [eV]. In both channels, new bands were created deep inside the MoS<sub>2</sub> band gap (between -0.02 and 0.48 [eV]) these new bands are responsible of the metallic behavior after the substitution.

Lastly, since the two-dimensional materials may be formed in heterostructures with no mismatch as discussed earlier. WSe<sub>2</sub> – MoS<sub>2</sub> (WSe<sub>2</sub> is another TMID's layered 2D material) heterostucture was investigated using LDA+U implemented in VASP, the band structure is shown in figure 28. The valence band maximum (VBM) was found to be 0.73 eV while the conduction band minimum (CBM) was 0.83 eV which is in agreement with the previous reported by Chiu et al.[56]. They found the VBM 0.76 and the CBM 0.83 eV. The band structure of MoS<sub>2</sub> was packed by bands, which I had to remove some to be able to interpret the structure.

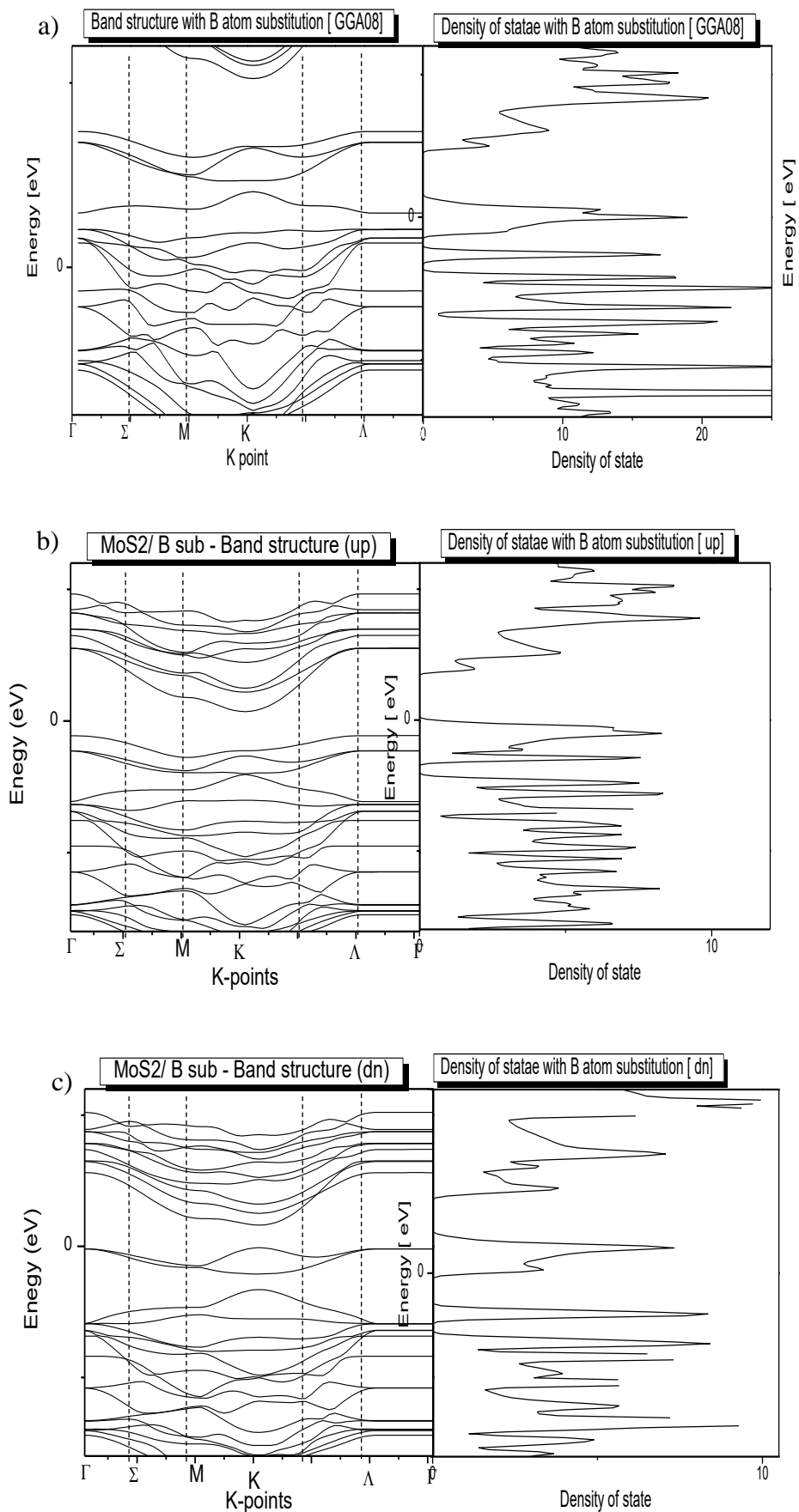


Figure 25: Band structure of ML MoS<sub>2</sub> with B substitution in Sulfur vacancy using a) GGA b) up spin channel c) down spin channel



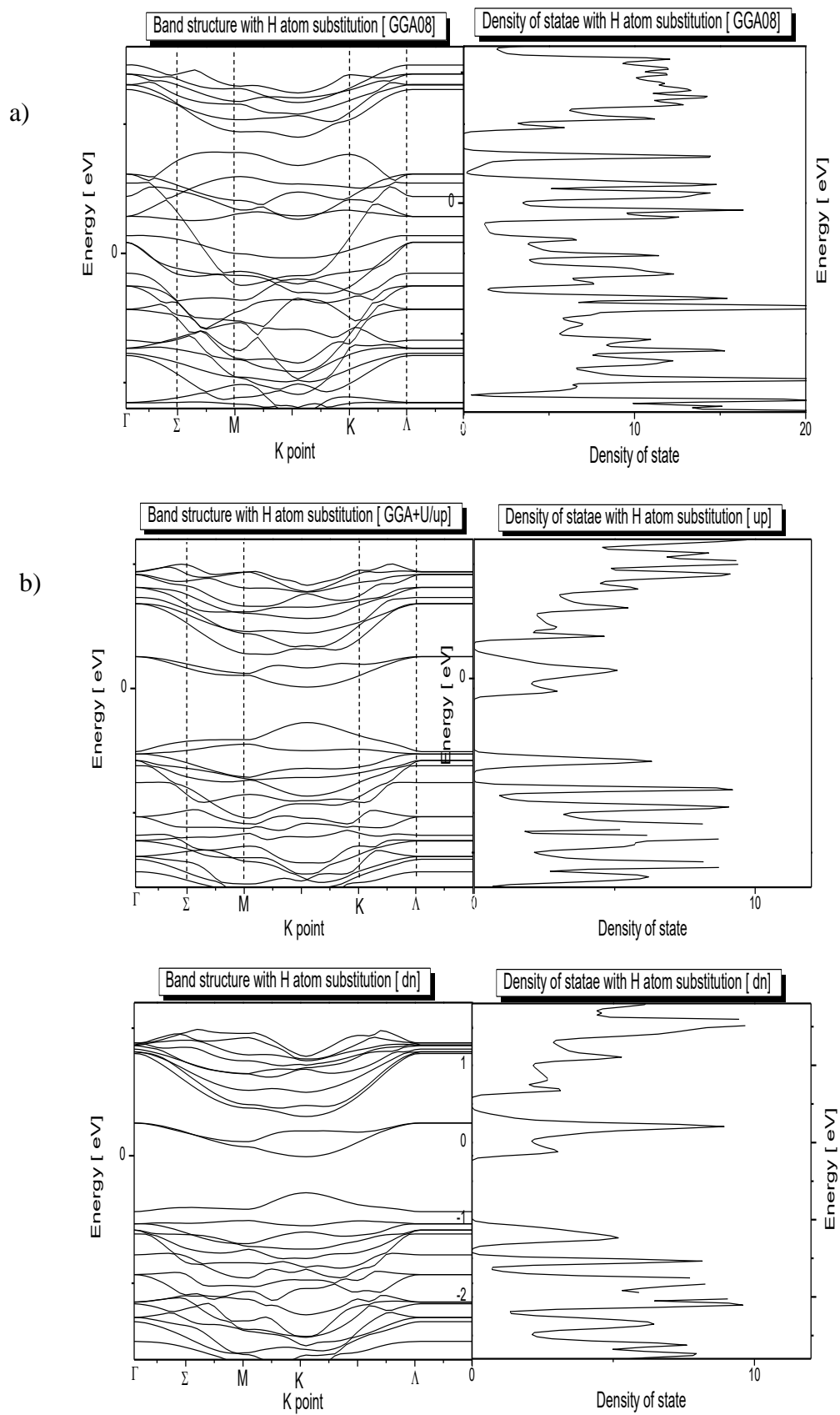


Figure 26: Band structure of ML MoS<sub>2</sub> with Hydrogen substitution in Sulfur vacancy using a) GGA b) up spin channel c) down spin channel

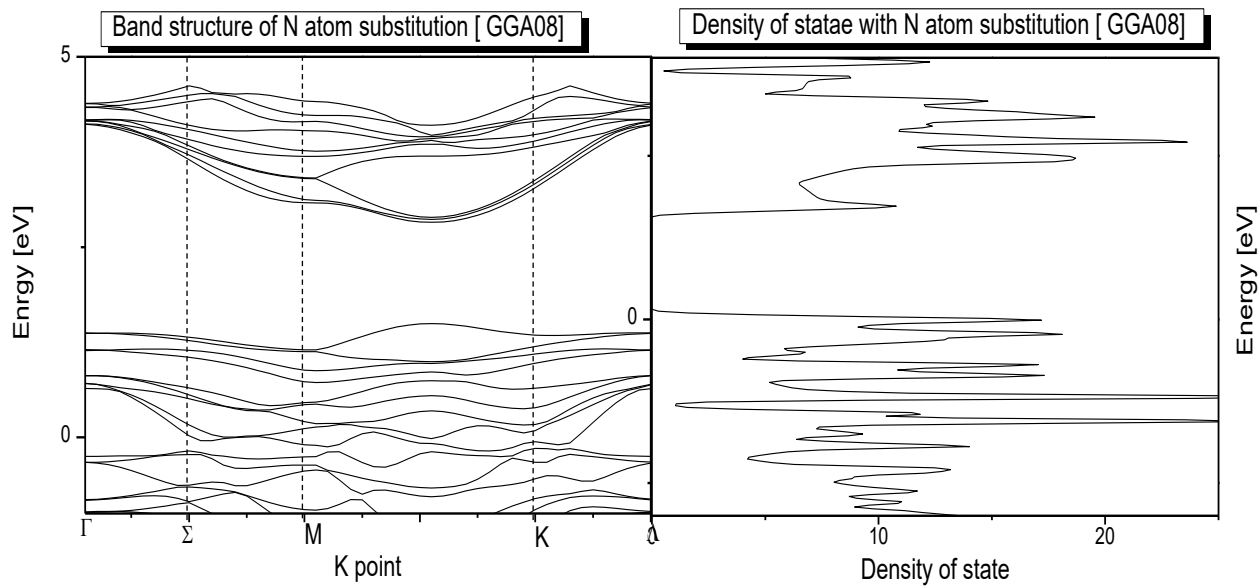


Figure 27: Band structure of monolayer  $\text{MoS}_2$  with Nitrogen substitution in Sulfur vacancy

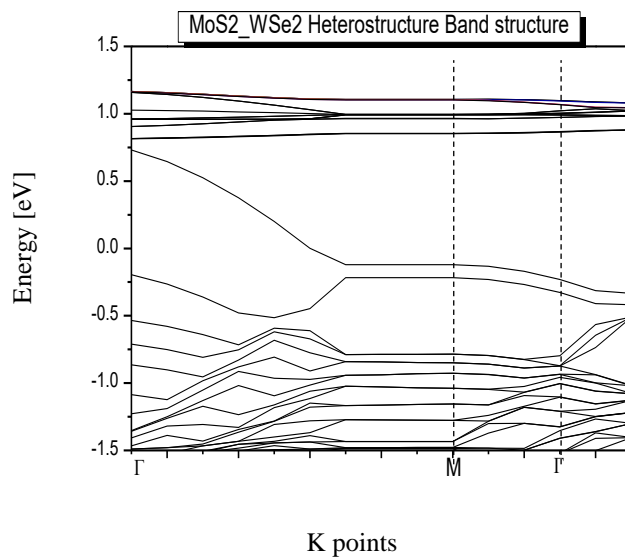


Figure 28: The band structure of  $\text{MoS}_2$ - $\text{WSe}_2$  using LDA+U

#### 5.4 Effect of Pressure on the Electronic Properties

Pressure investigation is essential to improve our understanding about many physical properties of the materials. In 2013 Bandaru *et al.* investigated the effect of pressure up to 51 GPa using Raman spectroscopy [57]. They showed that the diffraction pattern stays the same up to 23 GPa but at 26 GPa, the intensity of certain peaks dropped. At 17 GPa a new line emerges which suggests the presence of another phase. In 2014, Zhen-Hua Chi *et al.* proposed that inducing pressure is an excellent way to change the lattice without impurities intervention. They conducted their experiment using X ray diffraction, Raman spectroscopy and electrical conductivity measurements. They found that by increasing the pressure up to 20 GPa a new phase emerges (metallic phase) and appears along with the semiconductor phase until 40 GPa is reached where the transition is completed and MoS<sub>2</sub> becomes metallic [58]. They explained this transition by the collapse in the c-lattice constant, the volume and due to the interlayer bonding.

Following Bandaru and Chi work [57] [58], an investigation of the positive and negative pressure was induced using WIEN2K package within MBJ approximation. Pressure up to 50 GPa was applied on a bulk MoS<sub>2</sub> and as low as -30 GPa. The volume of MoS<sub>2</sub> changes while applying pressure as shown in figure 29. As experiments showed that, the band gap decreases with increasing pressure for the reasons stated by Chi *et al.* Figure 30 shows the behavior of the band gap with respect to pressure, which is consistent with the experimental results. A saturated region is observed beyond -25 GPa where the energy approximately stabilizes, it is important to note that the volume also will not vary if pressure was increased beyond -30 GPa (Unfortunately there is not much information in the literature regarding the negative pressure). The band gap

and the DOS for Negative pressure are shown in figures 31a and 31b respectively. The positive pressure induced band gap reduction is shown in the band structure and DOS in figures 32 and 33 respectively.

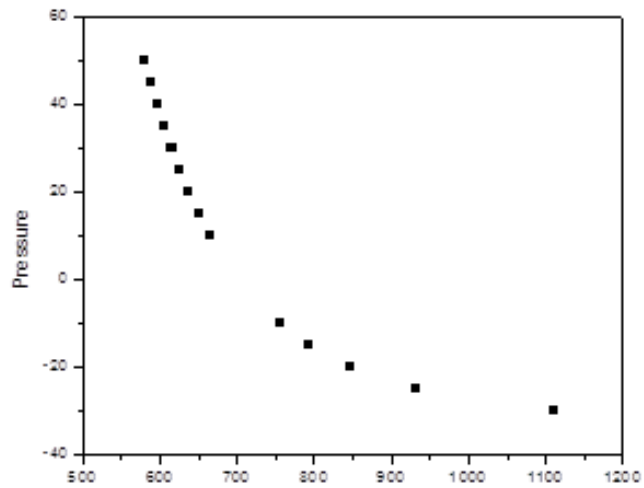


Figure 29: Behavior of the volume with respect to pressure

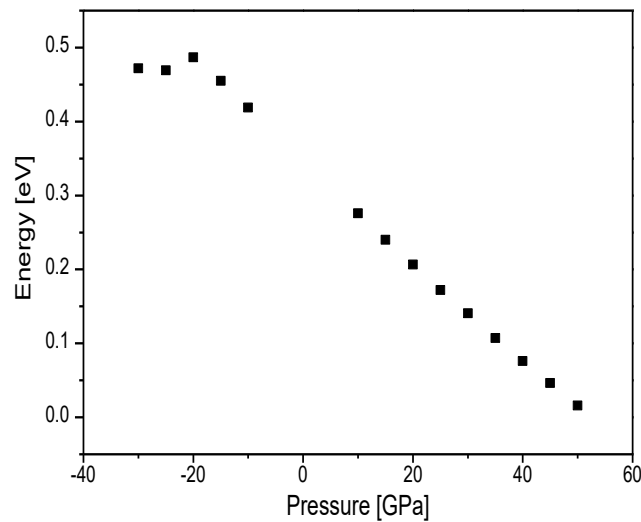


Figure 30: Behavior of the band gap with respect to pressure (While pressure increases the band gap decreases)

Table 10: Induced band gap reduction with increasing pressure. Pressure, Volume, lattice parameters and Band gap were calculated

<b>Pressure (GPa)</b>	<b>Volume (Bohr)<sup>3</sup></b>	<b>a(Bohr)</b>	<b>a,b (Å)</b>	<b>c(Å)</b>	<b>BG (eV)</b>
<b>-10</b>	755.6	6.218	3.23	11.724	0.41886
<b>-15</b>	793.8	6.32	3.286	11.928	0.45517
<b>-20</b>	846.8	6.46	3.359	12.193	0.48685
<b>-25</b>	930.8	6.661	3.464	12.52	0.46905
<b>-30</b>	1111.8	7.0717	3.677	13.35	0.47199
<b>10</b>	665.3	5.959	3.098	11.246	0.2758
<b>15</b>	650.49	5.915	3.076	11.165	0.23998
<b>20</b>	637.4	5.875	3.035	11.090	0.2067
<b>25</b>	625.71	5.837	3.019	11.017	0.172
<b>30</b>	615.15	5.806	3.003	10.959	0.1407
<b>35</b>	605.575	5.775	2.988	10.901	0.1073
<b>40</b>	596.79	5.747	2.9749	10.848	0.0761
<b>45</b>	588.7	5.721	2.962	10.799	0.0462
<b>50</b>	581.21	5.697	2.950	10.753	0.016

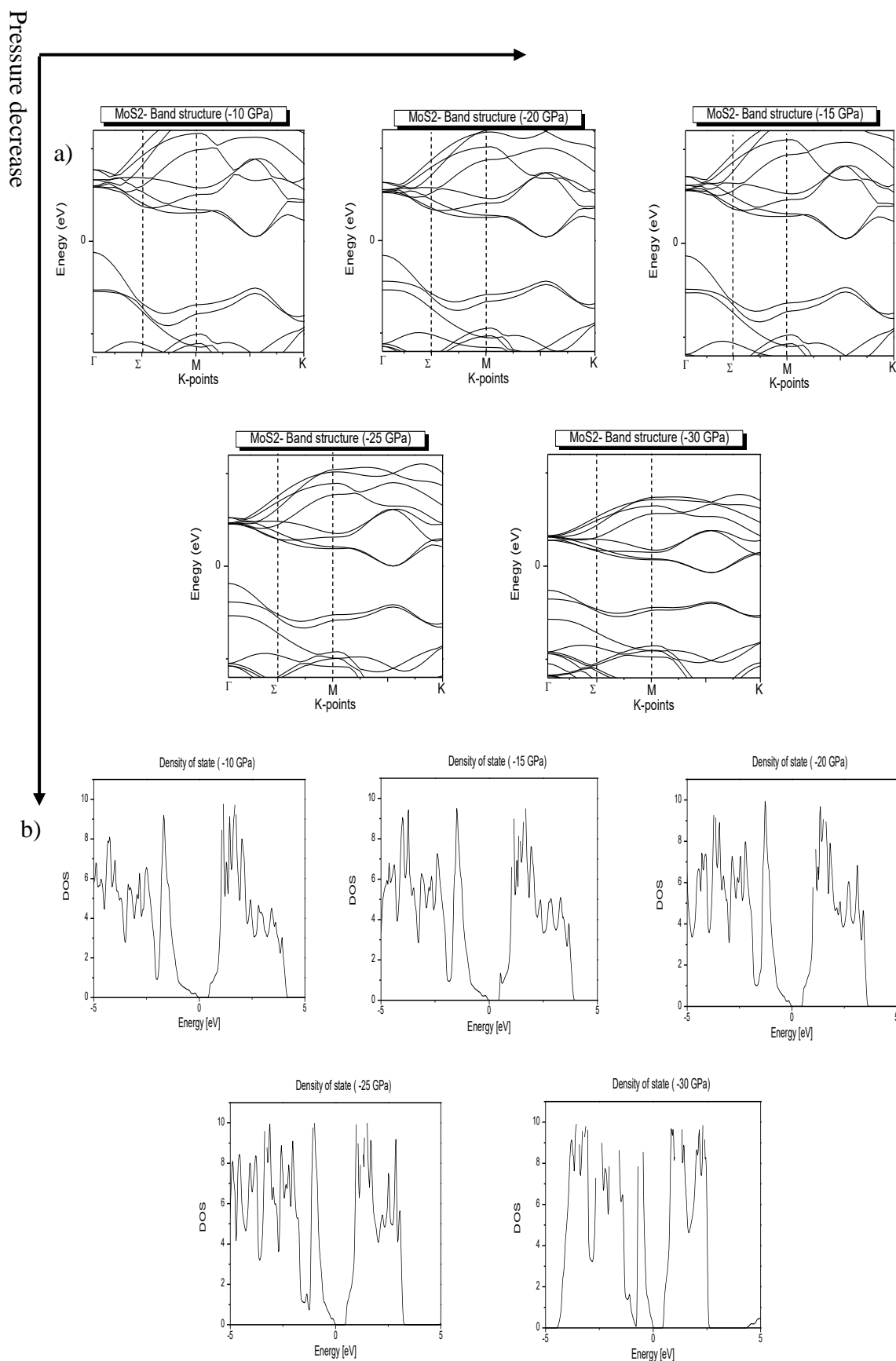


Figure 31: Effect of negative pressure a) The band structure of MoS<sub>2</sub> under negative pressure b) DOS of MoS<sub>2</sub> under negative pressure. The arrows shows the direction of decreasing pressure

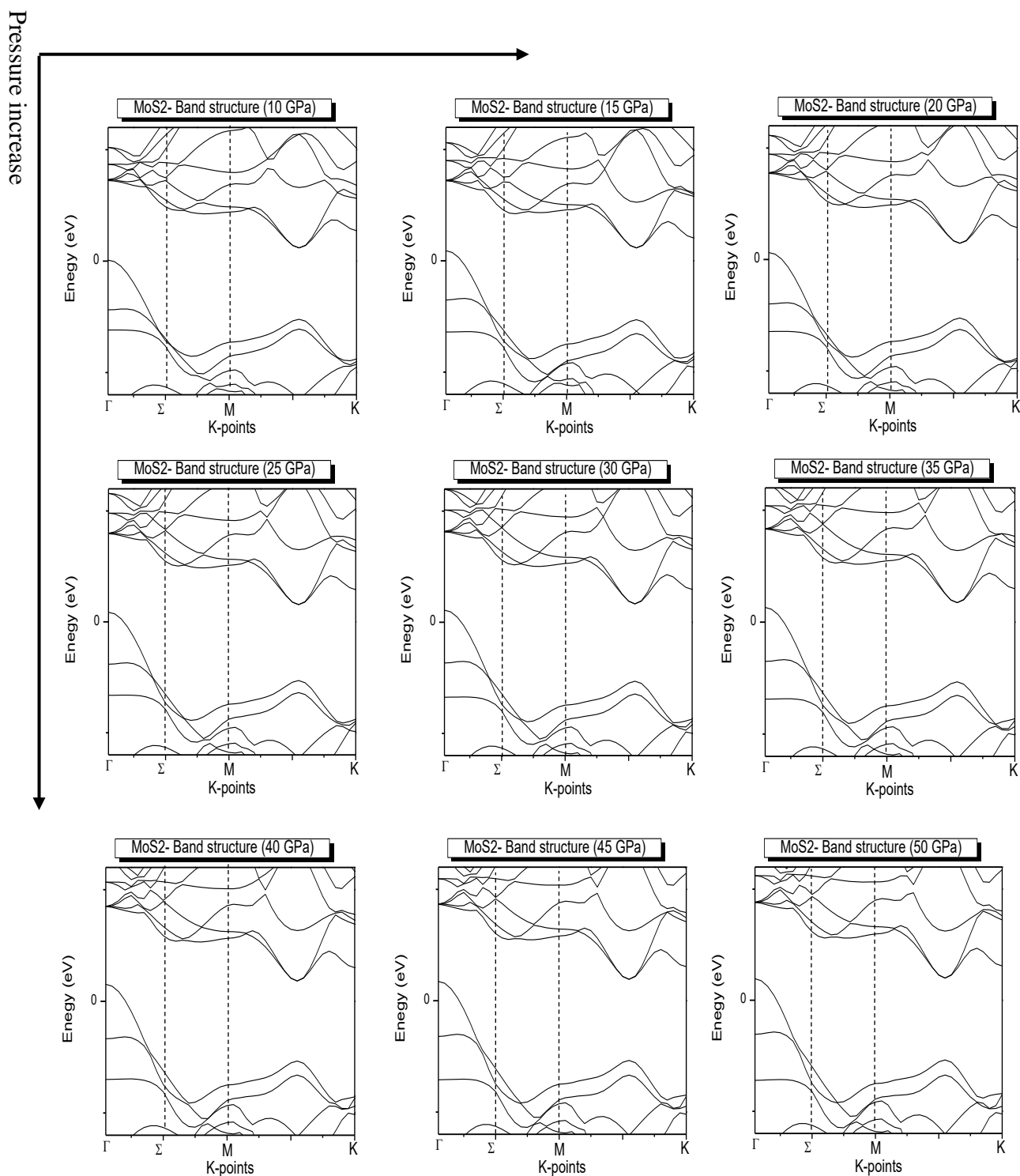


Figure 32: The band structure of MoS<sub>2</sub> under positive pressure. The arrows show the direction of increasing pressure

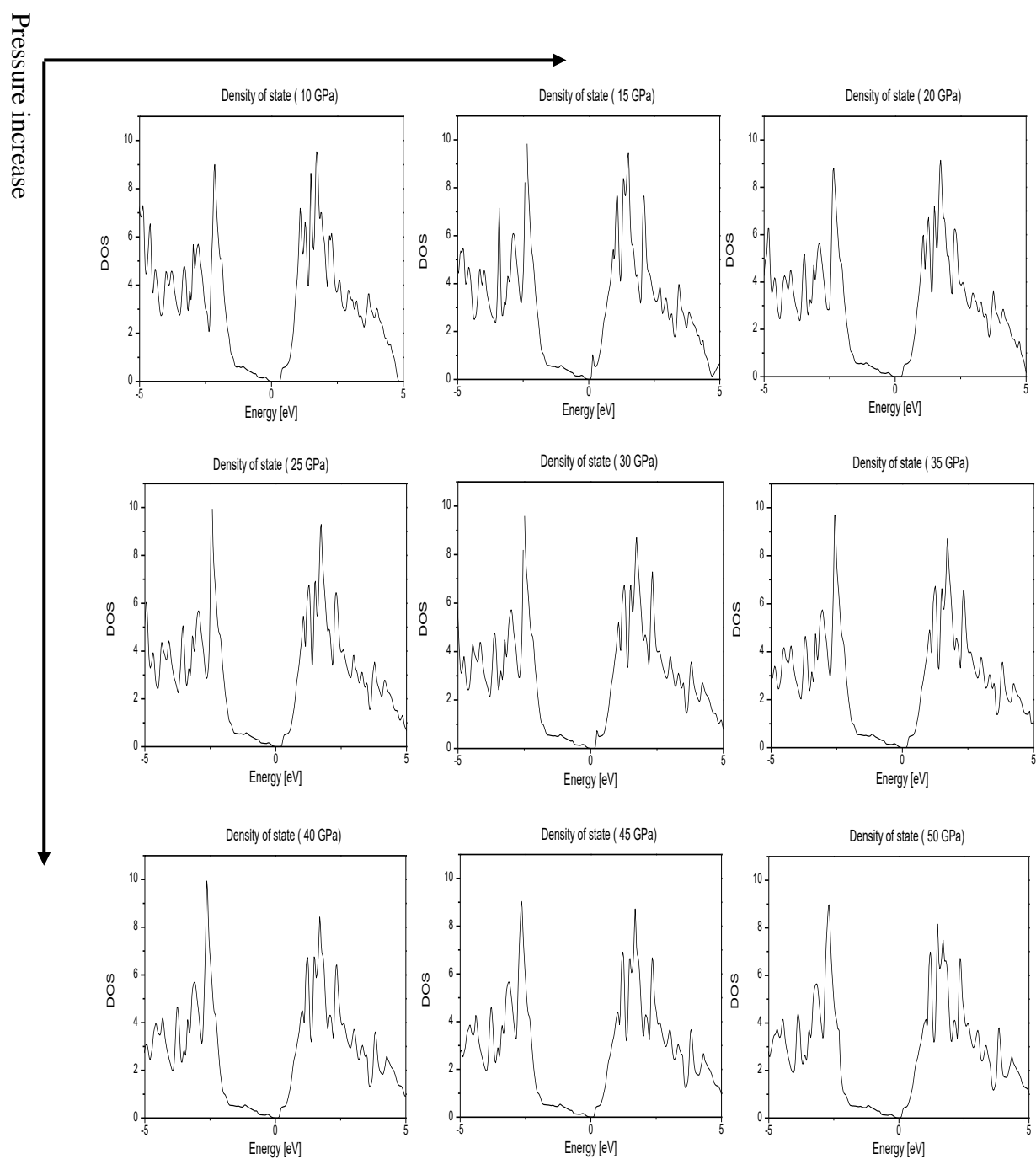


Figure 33: DOS of MoS<sub>2</sub> under positive pressure. The arrows show the direction of increasing pressure



## Chapter 6: Conclusion

Molybdenum disulfide is a promising class of material for next-generation electronics, as it is the only 2D material yet discovered which has an inherent band gap. It paves the way to a new generation of applications in the optical and electronic industry along its lubricant applications. In this approach, we used Generalized gradient approximation, Modified Becke Johnson, LDA+U and hybrid functional implemented in WIEN2k package and VASP (except MBJ in VASP) within DFT. We have shown that MoS<sub>2</sub> (an indirect band gap semiconductor), in its monolayer form, has a direct band gap (1.8eV) in the visible range (1.6-3.1 eV) which makes it an excellent candidate for optical applications and increases the possibility of creating an electron-hole pair. Our study shows that the manipulation of the monolayer MoS<sub>2</sub> band gap can be done using substitutional impurities and induced pressure and the metallization is possible which even widens the range of its applications. Metallizing partial size of the MoS<sub>2</sub> sample used for electronic applications where high conductivity and low resistivity are required.

We were limited by the size of our super-cells, bigger super cells would give even better results this is due to the insufficient computer capability (In order to study bigger supercells, super computers is needed).

Further investigation to find the effect of temperature and analyze the correlation between the two effects, pressure and temperature is recommended. Studying graphene- MoS<sub>2</sub> heterostructure is a very promising idea as well that is required for future applications.

## References

- [1] N. G. Chopra, R. J. Luyken, K. Cherrey, and V. H. Crespi, "Boron nitride nanotubes," *Science*, vol. 269, no. 5226, p. 966, 1995.
- [2] F. Xia, H. Wang, D. Xiao, M. Dubey, and A. Ramasubramaniam, "Two-dimensional material nanophotonics," *Nat. Photonics*, vol. 8, no. 12, pp. 899–907, 2014.
- [3] A. Shankara, P. L. Menezes, K. R. Y. Simha, and S. V. Kailas, "Study of solid lubrication with MoS<sub>2</sub> coating in the presence of additives using reciprocating ball-on-flat scratch tester," *Sadhana*, vol. 33, no. 3, pp. 207–220, 2008.
- [4] J.-Y. Wu, M.-N. Lin, L.-D. Wang, and T. Zhang, "Photoluminescence of MoS<sub>2</sub> prepared by effective grinding-assisted sonication exfoliation," *J. Nanomater.*, vol. 2014, p. 107, 2014.
- [5] Y. Tomm and S. Fiechter, "Crystal growth of materials for photovoltaics," *J. Ceram. Process. Res.*, vol. 6, no. 2, p. 141, 2005.
- [6] Y.-C. Lin, D. O. Dumcenco, Y.-S. Huang, and K. Suenaga, "Atomic mechanism of phase transition between metallic and semiconducting MoS<sub>2</sub> single-layers," *ArXiv Prepr. ArXiv13102363*, 2013.
- [7] D. Akinwande, N. Petrone, and J. Hone, "Two-dimensional flexible nanoelectronics," *Nat. Commun.*, vol. 5, 2014.
- [8] C. Lee, H. Yan, L. E. Brus, T. F. Heinz, J. Hone, and S. Ryu, "Anomalous lattice vibrations of single- and few-layer MoS<sub>2</sub>," *ACS Nano*, vol. 4, no. 5, pp. 2695–2700, 2010.
- [9] S. Sahoo, A. P. Gaur, M. Ahmadi, M. J.-F. Guinel, and R. S. Katiyar, "Temperature-dependent Raman studies and thermal conductivity of few-layer MoS<sub>2</sub>," *J. Phys. Chem. C*, vol. 117, no. 17, pp. 9042–9047, 2013.
- [10] X. Li and H. Zhu, "Two-dimensional MoS<sub>2</sub>: Properties, preparation, and applications," *J. Materiomics*, vol. 1, no. 1, pp. 33–44, 2015.
- [11] X. Li and H. Zhu, "Two-dimensional MoS<sub>2</sub>: Properties, preparation, and applications," *J. Materiomics*, vol. 1, no. 1, pp. 33–44, 2015.
- [12] Y. Ma, Y. Dai, W. Wei, C. Niu, L. Yu, and B. Huang, "First-principles study of the Graphene@ MoSe<sub>2</sub> heterobilayers," *J. Phys. Chem. C*, vol. 115, no. 41, pp. 20237–20241, 2011.
- [13] M. Bernardi, M. Palummo, and J. C. Grossman, "Extraordinary sunlight absorption and one nanometer thick photovoltaics using two-dimensional monolayer materials," *Nano Lett.*, vol. 13, no. 8, pp. 3664–3670, 2013.

- [14] K. Schwarz, "DFT calculations of solids with LAPW and WIEN2k," *J. Solid State Chem.*, vol. 176, no. 2, pp. 319–328, 2003.
- [15] C. D. Sherrill, "The born-oppenheimer approximation," *Sch. Chem. Biochem. Ga. Inst. Technol.*, 2005.
- [16] A. D. Becke, "Hartree–Fock exchange energy of an inhomogeneous electron gas," *Int. J. Quantum Chem.*, vol. 23, no. 6, pp. 1915–1922, 1983.
- [17] J. C. Slater, *The self-consistent field for molecules and solids*, vol. 4. McGraw-Hill New York, 1974.
- [18] J. C. Slater, *The self-consistent field for molecules and solids*, vol. 4. McGraw-Hill New York, 1974.
- [19] K. Burke, "The abc of dft," *Dep. Chem. Univ. Calif.*, 2007.
- [20] S. Cottenier, "Density Functional Theory and the family of (L) APW-methods: a step-by-step introduction," *Inst. Voor Kern-En Stralingsfysica KU Leuven Belg.*, vol. 4, no. 0, p. 41, 2002.
- [21] I. N. Levine, D. H. Busch, and H. Shull, *Quantum chemistry*, vol. 6. Pearson Prentice Hall Upper Saddle River, NJ, 2009.
- [22] W. Koch and M. C. Holthausen, *A chemist's guide to density functional theory*. John Wiley & Sons, 2015.
- [23] D. Sholl and J. A. Steckel, *Density functional theory: a practical introduction*. John Wiley & Sons, 2011.
- [24] E. Sjöstedt, L. Nordström, and D. J. Singh, "An alternative way of linearizing the augmented plane-wave method," *Solid State Commun.*, vol. 114, no. 1, pp. 15–20, 2000.
- [25] P. Blaha, K. Schwarz, P. Sorantin, and S. B. Trickey, "Full-potential, linearized augmented plane wave programs for crystalline systems," *Comput. Phys. Commun.*, vol. 59, no. 2, pp. 399–415, 1990.
- [26] G. Kresse and J. Furthmüller, "Efficiency of ab-initio total energy calculations for metals and semiconductors using a plane-wave basis set," *Comput. Mater. Sci.*, vol. 6, no. 1, pp. 15–50, 1996.
- [27] E. Y. Tsymbal, "Section 1-Crystal Structure (lecture notes)," *Solid-State Phys.*, vol. 927, pp. 1–9.
- [28] G. Schubert, J. Schleede, K. Byczuk, H. Fehske, and D. Vollhardt, "Distribution of the local density of states as a criterion for Anderson localization: Numerically exact results for various lattices in two and three dimensions," *Phys. Rev. B*, vol. 81, no. 15, p. 155106, 2010.

- [29] A. Wacker and M. Fysik, “An introduction to the concept of band structure,” 2017.
- [30] D. Neamen, *Semiconductor physics and devices*. McGraw-Hill, Inc., 2002.
- [31] M. Kuno, *Introductory Nanoscience*. Garland Science, 2011.
- [32] J. P. Perdew, “Generalized gradient approximations for exchange and correlation: A look backward and forward,” *Phys. B Condens. Matter*, vol. 172, no. 1–2, pp. 1–6, 1991.
- [33] K. Burke, J. P. Perdew, and M. Ernzerhof, “Why the generalized gradient approximation works and how to go beyond it,” *Int. J. Quantum Chem.*, vol. 61, no. 2, pp. 287–293, 1997.
- [34] K. A. BRUECKNER, “Correlation energy of an electron gas with a slowly varying high density,” *Phys. Rev.*, vol. 165, no. 1, p. 18, 1968.
- [35] Y. Zhang and W. Yang, “Comment on ‘Generalized gradient approximation made simple,’” *Phys. Rev. Lett.*, vol. 80, no. 4, p. 890, 1998.
- [36] J. P. Perdew, K. Burke, and M. Ernzerhof, “Generalized gradient approximation made simple,” *Phys. Rev. Lett.*, vol. 77, no. 18, p. 3865, 1996.
- [37] J. P. Perdew, K. Burke, and M. Ernzerhof, “Perdew, burke, and ernzerhof reply,” *Phys. Rev. Lett.*, vol. 80, no. 4, p. 891, 1998.
- [38] A. D. Becke, “Hartree–Fock exchange energy of an inhomogeneous electron gas,” *Int. J. Quantum Chem.*, vol. 23, no. 6, pp. 1915–1922, 1983.
- [39] D. Koller, F. Tran, and P. Blaha, “Merits and limits of the modified Becke–Johnson exchange potential,” *Phys. Rev. B*, vol. 83, no. 19, p. 195134, 2011.
- [40] A. D. Becke and E. R. Johnson, *A simple effective potential for exchange*. AIP, 2006.
- [41] J. C. Slater, “Magnetic effects and the Hartree-Fock equation,” *Phys. Rev.*, vol. 82, no. 4, p. 538, 1951.
- [42] J. P. Perdew and W. Yue, “Accurate and simple density functional for the electronic exchange energy: Generalized gradient approximation,” *Phys. Rev. B*, vol. 33, no. 12, p. 8800, 1986.
- [43] M. Cococcioni, “The LDA+ U Approach: A Simple Hubbard Correction for Correlated Ground States,” *Correl. Electrons Models Mater.*
- [44] M. Cococcioni and S. De Gironcoli, “Linear response approach to the calculation of the effective interaction parameters in the LDA+ U method,” *Phys. Rev. B*, vol. 71, no. 3, p. 035105, 2005.

- [45] J. Heyd, G. E. Scuseria, and M. Ernzerhof, “Hybrid functionals based on a screened Coulomb potential,” *J. Chem. Phys.*, vol. 118, no. 18, pp. 8207–8215, 2003.
- [46] K. Burke, M. Ernzerhof, and J. P. Perdew, “The adiabatic connection method: a non-empirical hybrid,” *Chem. Phys. Lett.*, vol. 265, no. 1–2, pp. 115–120, 1997.
- [47] J. Heyd and G. E. Scuseria, “Efficient hybrid density functional calculations in solids: assessment of the Heyd–Scuseria–Ernzerhof screened Coulomb hybrid functional,” *J. Chem. Phys.*, vol. 121, no. 3, pp. 1187–1192, 2004.
- [48] L. E. Ramos, J. Furthmüller, L. M. R. Scolfaro, J. R. Leite, and F. Bechstedt, “Substitutional carbon in group-III nitrides: Ab initio description of shallow and deep levels,” *Phys. Rev. B*, vol. 66, no. 7, p. 075209, 2002.
- [49] J. Hafner, “Materials simulations using VASP—a quantum perspective to materials science,” *Comput. Phys. Commun.*, vol. 177, no. 1, pp. 6–13, 2007.
- [50] Q. Yue, S. Chang, S. Qin, and J. Li, “Functionalization of monolayer MoS<sub>2</sub> by substitutional doping: a first-principles study,” *Phys. Lett. A*, vol. 377, no. 19, pp. 1362–1367, 2013.
- [51] T. Böker *et al.*, “Band structure of MoS<sub>2</sub>, MoSe<sub>2</sub>, and  $\alpha$ -MoTe<sub>2</sub>: Angle-resolved photoelectron spectroscopy and ab initio calculations,” *Phys. Rev. B*, vol. 64, no. 23, p. 235305, 2001.
- [52] J. A. Wilson and A. D. Yoffe, “The transition metal dichalcogenides discussion and interpretation of the observed optical, electrical and structural properties,” *Adv. Phys.*, vol. 18, no. 73, pp. 193–335, 1969.
- [53] K. F. Mak, C. Lee, J. Hone, J. Shan, and T. F. Heinz, “Atomically thin MoS<sub>2</sub>: a new direct-gap semiconductor,” *Phys. Rev. Lett.*, vol. 105, no. 13, p. 136805, 2010.
- [54] C. Kim *et al.*, “Fermi Level Pinning at Electrical Metal Contacts of Monolayer Molybdenum Dichalcogenides,” *ACS Nano*, vol. 11, no. 2, pp. 1588–1596, 2017.
- [55] J. He, K. Wu, R. Sa, Q. Li, and Y. Wei, “Magnetic properties of nonmetal atoms absorbed MoS<sub>2</sub> monolayers,” *Appl. Phys. Lett.*, vol. 96, no. 8, p. 082504, 2010.
- [56] M.-H. Chiu *et al.*, “Determination of band alignment in the single-layer MoS<sub>2</sub>/WSe<sub>2</sub> heterojunction,” *Nat. Commun.*, vol. 6, 2015.
- [57] N. Bandaru *et al.*, “Effect of pressure and temperature on structural stability of MoS<sub>2</sub>,” *J. Phys. Chem. C*, vol. 118, no. 6, pp. 3230–3235, 2014.
- [58] Z.-H. Chi *et al.*, “Pressure-induced metallization of molybdenum disulfide,” *Phys. Rev. Lett.*, vol. 113, no. 3, p. 036802, 2014.